UC San Diego
UC San Diego Previously Published Works

Title

A Multiwavenumber Theory for Eddy Diffusivities and Its Application to the Southeast Pacific (DIMES) Region

Permalink

https://escholarship.org/uc/item/8rs4f57d

Journal

Journal of Physical Oceanography, 45(7)

ISSN

0022-3670

Authors

Chen, Ru
Gille, Sarah T
McClean, Julie L
et al.

Publication Date

2015-07-01

DOI

10.1175/jpo-d-14-0229.1

Peer reviewed

A Multiwavenumber Theory for Eddy Diffusivities and Its Application to the Southeast Pacific (DIMES) Region

RU CHEN, SARAH T. GILLE, AND JULIE L. MCCLEAN

Scripps Institution of Oceanography, University of California, San Diego, La Jolla, California

GLENN R. FLIERL

Massachusetts Institute of Technology, Cambridge, Massachusetts

ALEXA GRIESEL

KlimaCampus, University of Hamburg, Germany

ABSTRACT

A multiwavenumber theory is formulated to represent eddy diffusivities. It expands on earlier single-wavenumber theories and includes the wide range of wavenumbers encompassed in eddy motions. In the limiting case in which ocean eddies are only composed of a single wavenumber, the multiwavenumber theory is equivalent to the single-wavenumber theory and both show mixing suppression by the eddy propagation relative to the mean flow. The multiwavenumber theory was tested in a region of the Southern Ocean (70°–45°S, 110°–20°W) that covers the Drake Passage and includes the tracer/float release locations during the Diapycnal and Isopycnal Mixing Experiment in the Southern Ocean (DIMES). Cross-stream eddy diffusivities and mixing lengths were estimated in this region from the single-wavenumber theory, from the multiwavenumber theory, and from floats deployed in a global $1/10°$ Parallel Ocean Program (POP) simulation. Compared to the single-wavenumber theory, the horizontal structures of cross-stream mixing lengths from the multiwavenumber theory agree better with the simulated float-based estimates at almost all depth levels. The multiwavenumber theory better represents the vertical structure of cross-stream mixing lengths both inside and outside the Antarctica Circumpolar Current (ACC). Both the single-wavenumber and multiwavenumber theories represent the horizontal structures of cross-stream diffusivities, which resemble the eddy kinetic energy patterns.

1. Introduction

Eddies are not explicitly resolved in standard-resolution, centennial-scale, global climate simulations; however, these simulations are sensitive to the representation of eddy mixing processes (e.g., Danabasoglu and Marshall 2007). This sensitivity has motivated efforts to estimate eddy mixing rates in the ocean that aim to reveal mixing processes leading to improved eddy parameterizations (e.g., Gille et al. 2012). Both float-based

and tracer-based diagnostic approaches have been employed to estimate diffusivities in the tropical North Atlantic (e.g., Banyte et al. 2013), western boundary currents (e.g., Chen et al. 2014), the Southern Ocean (e.g., LaCasce et al. 2014; Tulloch et al. 2014), and the global surface (e.g., Abernathey and Marshall 2013).

Understanding the estimated diffusivity patterns is a necessary step toward improving eddy parameterization schemes. A common approach is to interpret the mixing length L_{mix} instead of the diffusivity itself:

$$L_{\mathrm{mix}} = \frac{\kappa}{\Gamma u_{\mathrm{rms}}}, \qquad (1)$$

where Γ denotes the $O(1)$ mixing efficiency, u_{rms} is the eddy velocity magnitude, and κ denotes the

Corresponding author address: Ru Chen, Scripps Institution of Oceanography, University of California, San Diego, 9500 Gilman Dr., Mail Code 0230, La Jolla, CA 92093-0230.
E-mail: ruchen@alum.mit.edu

eddy diffusivity (e.g., Taylor 1915; Klocker and Abernathey 2014).

Bates et al. (2014) pointed out that ocean studies often assume that L_{mix} is of the same order of magnitude as the eddy size (e.g., Holloway 1986; Haine and Marshall 1998). This assumption is reasonable in an ocean without mean flows (Klocker and Abernathey 2014). In regions of the real ocean that contain mean flows, such as the Antarctica Circumpolar Current (ACC) and western boundary currents, eddy mixing in the cross-mean flow (cross stream) direction can be suppressed when eddies propagate relative to the mean flow. This concept dates back to Bretherton (1966) and Green (1970) and can be interpreted as follows: If eddies are stationary relative to the mean flow, eddies have sufficient time to stir and mix the same tracers, which also move with the mean flow; on the other hand, if the eddies propagate relative to the mean flow, eddies do not mix the same tracers, and mixing is suppressed (Klocker and Abernathey 2014). This idea has also recently been applied to studies about chaotic advection (Pratt et al. 2014).

Analytical formulas exist to represent the suppression of cross-stream mixing length by the eddy propagation relative to the mean flow (e.g., Green 1970; Killworth 1997; Ferrari and Nikurashin 2010; Klocker et al. 2012a). Ferrari and Nikurashin (2010) (F–N theory) proposed that the cross-stream mixing length $L_{mix,\perp}$ satisfies

$$L_{mix,\perp} = \frac{L}{1 + k_{eddy}^2 \gamma^{-2}(C_w - |\mathbf{U}|)^2}, \qquad (2)$$

where $|\mathbf{U}|$ denotes the mean flow magnitude. Note that although some previous studies (e.g., Klocker and Abernathey 2014) assume that the mean flow is zonal, this theory applies to the case with the mean flow in any arbitrary direction (Chen et al. 2014). Here, C_w denotes the phase speed along the mean flow direction; positive C_w corresponds to downstream propagation, and negative C_w corresponds to upstream propagation (Chen et al. 2014). The terms k_{eddy}, L, and γ are the eddy wavenumber, eddy length scale, and the reciprocal of eddy decorrelation time, respectively. Surface eddy diffusivities from the F–N theory agree with those from altimetry (e.g., Ferrari and Nikurashin 2010; Klocker and Abernathey 2014; Bates et al. 2014). The F–N theory also captures the three-dimensional structure of float-based eddy diffusivities in the intense Kuroshio Extension jet area (Chen et al. 2014). On the other hand, the theory appears to break down in regions where large topographic gradients occur (e.g., Griesel et al. 2010; Naveira-Garabato et al. 2011; Chen et al. 2014). Bates et al. (2014) found that the F–N theory is also not effective in capturing the observed vertical structures of

eddy diffusivities from the U.S./U.K. field program Diapycnal and Isopycnal Mixing Experiment in the Southern Ocean (DIMES; e.g., Ledwell et al. 2011) or from the North Atlantic Tracer Release Experiment (NATRE; e.g., Ledwell et al. 1998).

The breakdown of the F–N theory in some ocean scenarios is unsurprising, considering that it is built on a number of assumptions that are violated in the ocean, including a flat bottom, a spatially and temporally constant mean flow, and scale separation between the mean flow and eddies (e.g., Ferrari and Nikurashin 2010). One assumption upon which these theories, including the F–N theory, are based is that eddies only contain a single wave corresponding to the most unstable mode or that eddies are dominated by a single wave (e.g., Green 1970; Killworth 1997; Ferrari and Nikurashin 2010; Klocker et al. 2012a). In fact, the frequency–wavenumber spectra of sea surface height is a broad continuum with no robust peaks, indicating that the oceanic eddy field includes motions over a broad range of wavenumbers and frequencies (e.g., Wunsch 2010; Wortham 2013; Wortham and Wunsch 2014). Even a single Gaussian vortex can be decomposed into wave motions with a range of wavenumbers and frequencies (Chen et al. 2015). In the midlatitude ocean interior away from western boundary currents, the phase speeds for all the dominant wavenumbers are roughly the same; however, in the Gulf Stream, the Kuroshio Extension, and the ACC, the dominant waves are dispersive, and both eastward- and westward-propagating waves are nonnegligible [see Figs. 2–16 in Wortham (2013)].

Assuming that internal waves are small-amplitude Gaussian random processes, Holmes-Cerfon et al. (2011) developed a formula for one-particle horizontal diffusivity based on the internal wave spectra. Feddersen (2004) found that estimates of radiation stresses based on full spectra are different from those based on a peak frequency. Inspired by Holmes-Cerfon et al. (2011) and Feddersen (2004), and motivated by the discrepancy between the single-wavenumber assumption and the observed broadbanded oceanic spectra, here we formulate a multiwavenumber theory (MW theory) for eddy diffusivities in the mean flow (section 2). The theory can be derived from both float-based and tracer-based diffusivity formulas (sections 2a and 2b), and it links diffusivities with the frequency–wavenumber spectra of the Eulerian eddy velocity fields.

We choose the DIMES region (70°–45°S, 110°–20°W) as a test bed for the MW theory (Fig. 1). It covers both the region upstream of the Drake Passage, where the floats and tracers were released in the DIMES experiment (e.g., Ledwell et al. 2011; Watson et al. 2013; Sheen et al. 2013; LaCasce et al. 2014; Tulloch et al. 2014), and the region downstream of the Drake Passage (Scotia
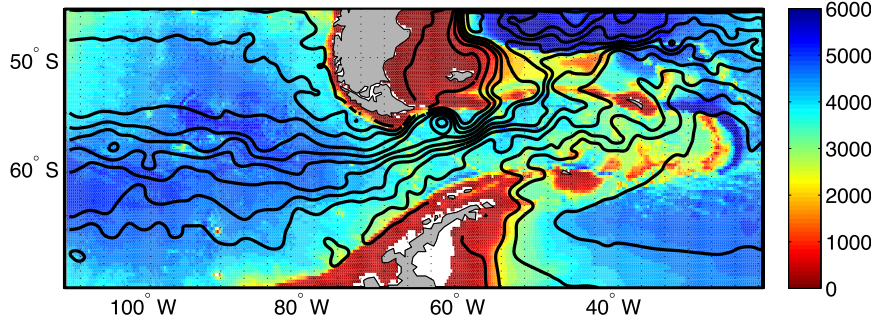
FIG. 1. Bathymetry (color; m) and barotropic streamlines (black contours) from the POP model in our study domain. Barotropic streamlines here and in the following figures are defined as $\psi_g = g f^{-1} \overline{\eta}$, where f is the Coriolis parameter and $\overline{\eta}$ is the sea surface height averaged over the years 1994–95.

Sea), where eddy kinetic energy is larger and mixing is more intense than upstream of the Drake Passage. Eddy diffusivities are estimated at high spatial resolution from numerical floats deployed in a global eddying model. These float-based diffusivities are used not only to test the relevance of the single-wavenumber and multi-wavenumber theories but also to help put the sparse mixing observations in the DIMES region into a larger spatial context.

This paper is organized as follows: Section 2 introduces the MW theory of eddy diffusivities and illustrates its consistency with the F–N theory in the single-wavenumber limit. Section 3 describes the configuration of the global eddying model with numerical floats, which we use to test the applicability of our theory. Section 4 presents eddy diffusivities in the DIMES area from the numerical floats in the eddying model. Section 5 provides the diffusivities diagnosed from both the F–N and MW theories and compares them with the float-based diffusivities. Sections 6 and 7 provide the discussion and summary, respectively.

2. The multiwavenumber theory from both float and tracer perspectives

Here, we derive the MW theory for the diffusivity tensor and cross-stream diffusivities from both the float and tracer perspectives. Its consistency with the F–N theory in the single-wavenumber scenario is demonstrated in appendix A.

a. The multiwavenumber theory derived from Lagrangian eddy diffusivities

1) DIFFUSIVITY TENSOR IN AUTOCORRELATION FORM

Lagrangian eddy diffusivities can be estimated from numerical floats. We start from the diagnostic formulas,

involving the integral over the autocovariance function (Davis 1991; Griesel et al. 2010, 2014; Chen et al. 2014):

$$\kappa_{ij}^{L,\infty}(\mathbf{x}) = \lim_{\tau \to \infty} \kappa_{ij}^{L}(\mathbf{x}, \tau)$$

$$= \lim_{\tau \to \infty} \int_0^\tau d\tilde{\tau} \langle u_{i,L}'(t_0 \,|\, \mathbf{x}, t_0) u_{j,L}'(t_0 + \tilde{\tau} \,|\, \mathbf{x}, t_0) \rangle, \quad (3)$$

where $\kappa_{ij}^{L,\infty}(\mathbf{x})$ is the value of the diffusivity tensor $\kappa_{ij}^{L}(\mathbf{x}, \tau)$ in the limit as time lag τ goes to infinity and $\langle \cdot \rangle$ denotes the ensemble average of many pseudo float trajectories with center positions passing $\mathbf{x}$. Here, $u_{i,L}'(t_0 + \tau \,|\, \mathbf{x}, t_0)$ denotes the residual velocity in the i direction at time $t_0 + \tau$ for the float that passes position $\mathbf{x}$ at time t_0. Residual velocities denote the float velocities subtracted from the local "time-mean" Eulerian velocity at the float position.

Following Klocker et al. (2012a), we assume that (i) the mean flow varies on spatial scales larger than eddies, and thus the mean flow vector $\mathbf{U}$ is approximately a constant, and (ii) the eddy velocity magnitude is much smaller than the mean flow magnitude. Therefore, to leading order, floats move only with the mean flow. Consequently, the Lagrangian velocities $u_{i,L}'$ can be obtained from the Eulerian velocities:

$$u_{i,L}'(t_0 \,|\, \mathbf{x}, t_0) = u_i'(\mathbf{x}, t_0), \quad \text{and}$$
$$u_{i,L}'(t_0 + \tilde{\tau} \,|\, \mathbf{x}, t_0) = u_i'(\mathbf{x} + \mathbf{U}\tilde{\tau}, t_0 + \tilde{\tau}), \quad (4)$$

where u_i' denotes the Eulerian eddy velocities in the i direction.

Following Klocker et al. (2012a), we set the starting time of the float t_0 to be zero, without loss of generality. Then substituting Eq. (4) into Eq. (3),

$$\kappa_{ij}^{L,\infty}(\mathbf{x}) = \lim_{\tau \to \infty} \int_0^\tau d\tilde{\tau} \langle u_i'(\mathbf{x} + \mathbf{U}t, t)|_{t=0} \, u_j'(\mathbf{x} + \mathbf{U}t, t)|_{t=\tilde{\tau}} \rangle.$$

$$(5)$$

We define the Eulerian eddy velocities at position $\mathbf{x} + \mathbf{U}t$ at time t as

$$\mathcal{U}'_i(\mathbf{x}, t) = u'_i(\mathbf{x} + \mathbf{U}t, t); \quad (6)$$

then we obtain from Eq. (5)

$$\kappa_{ij}^{L,\infty}(\mathbf{x}) = \lim_{\tau \to \infty} \int_0^\tau d\tilde{\tau} \langle \mathcal{U}'_i(\mathbf{x}, t)|_{t=0} \mathcal{U}'_j(\mathbf{x}, t)|_{t=\tilde{\tau}} \rangle. \quad (7)$$

Assuming that the eddy statistics are temporally stationary, we have

$$\kappa_{ij}^{L,\infty}(\mathbf{x}) = \frac{1}{2} \lim_{\tau \to \infty} \int_{-\tau}^\tau d\tilde{\tau} \langle \mathcal{U}'_i(\mathbf{x}, t)|_{t=0} \mathcal{U}'_j(\mathbf{x}, t)|_{t=\tilde{\tau}} \rangle. \quad (8)$$

2) DIFFUSIVITY TENSOR IN SPECTRAL FORM

The derivation so far is similar to that of Klocker et al. (2012a), who provided a derivation for the F–N theory from the Lagrangian perspective. The second part of the derivation (in this subsection) diverges from Klocker et al. (2012a) in order to develop a multiwavenumber mixing formula. Using the one-dimensional cross-correlation theorem (e.g., Weisstein 2014), Eq. (8) leads to

$$\kappa_{ij}^{L,\infty}(\mathbf{x}) = \frac{1}{2} \lim_{\omega' \to 0} \left\langle \widehat{\mathcal{U}'_i}(\omega') \widehat{\mathcal{U}'^*_j}(\omega') \right\rangle$$

$$\approx \frac{1}{2} \left\langle \widehat{\mathcal{U}'_i}(0) \widehat{\mathcal{U}'^*_j}(0) \right\rangle = \frac{1}{2} S_{\mathcal{U}'_i, \mathcal{U}'_j}(\omega', \mathbf{x}) \bigg|_{\omega'=0}, \quad (9)$$

where $\hat{\cdot}$ is the Fourier transform, $\cdot^*$ denotes the complex conjugate, and ω' denotes frequency. Because the Fourier transform of a real variable is real at zero frequency, $\langle \widehat{\mathcal{U}'_i}(0) \widehat{\mathcal{U}'^*_j}(0) \rangle$ is real, even when i and j differ. Following Randel and Held (1991), the one-dimensional cross spectrum of variables α and β at position $\mathbf{x}$, $S_{\alpha,\beta}(\omega', \mathbf{x})$, is defined as

$$S_{\alpha,\beta}(\omega', \mathbf{x}) = \text{Re}\langle \hat{\alpha}(\omega') \hat{\beta}^*(\omega') \rangle. \quad (10)$$

Following conventional notation (e.g., Ferrari and Wunsch 2010), we then define $S_{\alpha,\beta}(k', l', \omega', \mathbf{x})$ as the three-dimensional cross spectrum in an oceanic patch centered at $\mathbf{x}$:

$$S_{\alpha,\beta}(k', l', \omega', \mathbf{x}) = \text{Re}\langle \hat{\alpha}(k', l', \omega') \hat{\beta}^*(k', l', \omega') \rangle. \quad (11)$$

Here, we use a rotated, coordinate system with wavenumber l' perpendicular to the mean flow and wavenumber k' aligned with and pointing in the mean flow direction.

To obtain enough ensembles (float trajectories), we often estimate diffusivities averaged over a selected oceanic patch (using either geographic or adaptive bins) rather than carrying out a pointwise estimate. The spatial average of the one-dimensional spectra over the oceanic patch can be obtained from the three-dimensional spectra:

$$\overline{S_{\alpha,\beta}(\omega', \mathbf{x})}^{\text{patch}} = \int_{-\infty}^\infty \int_{-\infty}^\infty S_{\alpha,\beta}(k', l', \omega', \mathbf{x}) \, dk' \, dl', \quad (12)$$

where $\overline{\cdot}^{\text{patch}}$ denotes the spatial average over the patch. Equations (9) and (12) lead to the diffusivity tensor averaged over the selected oceanic patch centered at $\mathbf{x}$:

$$\overline{\kappa_{ij}^{L,\infty}(\mathbf{x})}^{\text{patch}} = \frac{1}{2} \int_{-\infty}^\infty \int_{-\infty}^\infty S_{\mathcal{U}'_i, \mathcal{U}'_j}(k', l', \omega', \mathbf{x})|_{\omega'=0} \, dk' \, dl'. \quad (13)$$

In practice, $\overline{\kappa_{ij}^{L,\infty}(\mathbf{x})}^{\text{patch}}$ is more easily diagnosed from the Eulerian eddy velocities u'_i rather than from $\mathcal{U}'_i$. Using the spectral analysis technique of Chen et al. (2015), we obtain from Eq. (6)

$$\widehat{\mathcal{U}'_i}(k', l', \omega') = \widehat{u'_i}(k', l', \omega' + |\mathbf{U}|k'), \quad (14)$$

where $|\mathbf{U}|$ is the magnitude of the mean flow vector $\mathbf{U}$, k' is the wavenumber in the direction of $\mathbf{U}$, and l' is the wavenumber perpendicular to $\mathbf{U}$. Therefore,

$$S_{\mathcal{U}'_i \mathcal{U}'_j}(k', l', \omega', \mathbf{x}) = S_{u'_i u'_j}(k', l', \omega' + |\mathbf{U}|k', \mathbf{x}). \quad (15)$$

Substituting Eq. (15) into Eq. (13) leads to our multiwavenumber formula for the diffusivity tensor averaged over the patch, involving the three-dimensional spectrum of Eulerian eddy velocities at the patch:

$$\overline{\kappa_{ij}^{L,\infty}(\mathbf{x})}^{\text{patch}} = \frac{1}{2} \int_{-\infty}^\infty \int_{-\infty}^\infty S_{u'_i u'_j}(k', l', |\mathbf{U}|k', \mathbf{x}) \, dk' \, dl'. \quad (16)$$

Using the above procedure, we can also obtain the diffusivity tensor averaged along a slice aligned with the mean flow direction and centered at $\mathbf{x}$ (see Fig. 7c):

$$\overline{\kappa_{ij}^{L,\infty}(\mathbf{x})}^{\text{slice}} = \frac{1}{2} \int_{-\infty}^\infty S_{u'_i u'_j}(k', |\mathbf{U}|k', \mathbf{x}) \, dk', \quad (17)$$

where $\overline{\cdot}^{\text{slice}}$ denotes the average along the slice, and $S_{u'_i u'_j}(k', \omega', \mathbf{x})$ is the two-dimensional cross spectrum along the slice.

3) CROSS-STREAM DIFFUSIVITIES IN SPECTRAL FORM

The full diffusivity tensor has received much attention in eddy parameterizations and tracer transport studies (e.g., Plumb and Mahlman 1987; Griffies 1998; Bachman

and Fox-Kemper 2013). However, previous investigations of the role of the mean flow in mixing have focused primarily on cross-stream mixing (e.g., Ferrari and Nikurashin 2010; Griesel et al. 2014), which drives the eddy-induced meridional overturning circulation in the Southern Ocean (Tulloch et al. 2014). For consistency with recent work on cross-stream mixing, we next present cross-stream diffusivities in spectral form. Subsequent sections focus on testing the validity of the MW theory in representing cross-stream diffusivities. For brevity, in this paper we will not discuss the full diffusivity tensor.

When the i and j components in Eq. (3) both represent the cross-stream direction, we obtain the float-based formula for cross-stream eddy diffusivities:

$$\kappa_\perp^{L,\infty}(\mathbf{x}) = \lim_{\tau \to \infty} \kappa_\perp(\mathbf{x}, \tau)$$
$$= \lim_{\tau \to \infty} \int_0^\tau d\tilde{\tau} \langle u'_{\perp,L}(t_0 \mid \mathbf{x}, t_0) u'_{\perp,L}(t_0 + \tilde{\tau} \mid \mathbf{x}, t_0) \rangle,$$
$$(18)$$

where $u'_{\perp,L}(t_0 + \tau \mid \mathbf{x}, t_0)$ denotes the residual velocity in the cross-stream direction at time $t_0 + \tau$ for the float that passes position $\mathbf{x}$ at time t_0.

Following sections 2a(1) and 2a(2), one can easily obtain cross-stream diffusivities in spectral form, again by using cross-stream components for both the i and j direction in Eqs. (16) and (17). The cross-stream diffusivity averaged over the patch centered at $\mathbf{x}$ is

$$\overline{\kappa_\perp^{L,\infty}(\mathbf{x})}^{\text{patch}} = \frac{1}{2} \int_{-\infty}^\infty \int_{-\infty}^\infty S_{u'_\perp, u'_\perp}(k', l', |\mathbf{U}|k', \mathbf{x}) \, dk' \, dl',$$
$$(19)$$

where $S_{u'_\perp, u'_\perp}(k', l', \omega', \mathbf{x})$ is the three-dimensional spectrum of the cross-stream Eulerian eddy velocities over the patch. Similarly, the cross-stream diffusivity averaged over a slice aligned with the mean flow direction and centered at $\mathbf{x}$ is

$$\overline{\kappa_\perp^{L,\infty}(\mathbf{x})}^{\text{slice}} = \frac{1}{2} \int_{-\infty}^\infty S_{u'_\perp, u'_\perp}(k', |\mathbf{U}|k', \mathbf{x}) \, dk', \quad (20)$$

where $S_{u'_\perp, u'_\perp}(k', \omega', \mathbf{x})$ is the two-dimensional spectrum of cross-stream Eulerian eddy velocities along the slice. Since $\overline{\kappa_\perp^{L,\infty}(\mathbf{x})}^{\text{slice}}$ has a higher cross-stream resolution than $\overline{\kappa_\perp^{L,\infty}(\mathbf{x})}^{\text{patch}}$, we diagnose $\overline{\kappa_\perp^{L,\infty}(\mathbf{x})}^{\text{slice}}$ in section 5. This will be denoted by $\kappa_\perp^{\text{multi}}$ for short.

We find that the MW theory is a natural extension of the single-wavenumber theory to a more realistic regime with multiple wavenumbers. As shown in appendix A, in the limit of a single wavenumber, cross-stream diffusivities from the MW theory reduce to the diffusivities from the single-wavenumber F–N theory.

b. The multiwavenumber theory derived from Eulerian eddy diffusivities

We can also obtain the MW theory for diffusivities presented in section 2a from an Eulerian diffusivity perspective. The tracer concentration C satisfies

$$\frac{\partial}{\partial t} C + \mathbf{u} \cdot \nabla C - \kappa_0 \nabla^2 C = 0, \quad (21)$$

where $\mathbf{u}$ is the total velocity, and κ_0 is the molecular or numerical diffusivity of the tracer. The Eulerian eddy diffusivity tensor κ_{ij}^{E} is often defined as

$$\overline{u_i' C'} = -\kappa_{ij}^{\text{E}} \frac{\partial}{\partial x_j} \overline{C}, \quad (22)$$

where the overbar denotes the ensemble average, the prime represents the deviation from the ensemble average, and u_i is the Eulerian velocity (e.g., Plumb and Mahlman 1987).

Consider the scenario from section 2a: eddies are of small amplitude compared to the mean flow and the system is spatially homogenous, with the spatial scale of the mean (e.g., mean flow and mean eddy flux) much larger than the eddy scale. Appendix B shows that κ_{ij}^{E} in this scenario is equivalent to the multiwavenumber diffusivity tensor derived from the Lagrangian perspective [Eqs. (16) and (17)], when κ_0 is very small.

3. Testing the theory: A global eddying model with numerical floats

We use a global eddying model to test whether the MW theory from section 2 can capture diffusivity structures in realistic contexts. The Parallel Ocean Program (POP) simulation used in this study is the same as that described by Chen et al. (2014). Here, we briefly review the key model features. The domain is global and the grid has a nominal spatial resolution of $1/10°$. In the vertical direction, the model is discretized into 42 vertical levels, and the layer thickness decreases from 10 m at the surface to 250 m at the ocean bottom. The K-profile parameterization (Large et al. 1994) is used to represent vertical mixing in the upper ocean, and biharmonic viscosity and diffusion parameterize horizontal mixing of momentum and tracers at subgrid scales.

As summarized by Abernathey et al. (2013), a number of methods exist for estimating eddy diffusivities. Here, we estimate Lagrangian eddy diffusivities from numerical floats (e.g., Davis 1987, 1991; Griesel et al. 2010). We deployed one million numerical floats at the beginning of
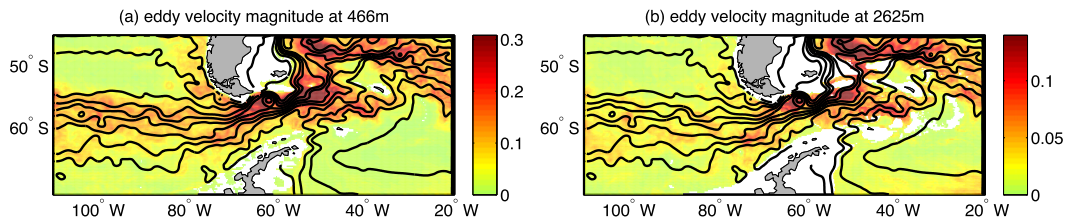
FIG. 2. Eddy velocity magnitude ($\sqrt{u'^2 + v'^2}$; m s^{-1}) at (a) 466 and (b) 2625 m from the POP model. The barotropic streamlines are superimposed as black contours to indicate the location of the ACC. Here, u' and v' are the deviation of total Eulerian velocity from the 2-yr (1994-95) mean.

the year 1994 uniformly over the entire globe at 23 vertical levels with a horizontal resolution of 0.25° in latitude and 2.5° in longitude. These floats were advected online by the three-dimensional Eulerian velocity fields for a full year. The float properties, including position, velocity, and density, were recorded at daily intervals.

Figure 1 shows our study domain, which extends from 70° to 45°S and from 110° to 20°W, roughly corresponding to the DIMES region. The barotropic streamlines, defined as $\psi_g = gf^{-1}\overline{\eta}$, are used as an indicator of the location of the time-mean ACC. Here, f is the Coriolis parameter, g is gravity, and $\overline{\eta}$ is the temporally averaged sea surface height over the years 1994–95. The time-mean ACC is broad and roughly zonal west of Drake Passage. Once inside Drake Passage, it intensifies because of mass conservation; it then shifts northward to the east of Drake Passage and becomes more spatially variable. Topographic variations are larger to the east of Drake Passage than they are to the west (Fig. 1). Figure 2 shows the eddy velocity magnitude at two selected depths. Though the eddy velocity magnitude gradually decreases with depth, its horizontal structures vary little with depth, with large magnitudes inside the ACC core.

The model agrees with observations and previous literature in the following two ways: First, the small change in horizontal structure with depth, shown in Fig. 2, is consistent with an equivalent barotropic flow field in the Southern Ocean, as has been identified and employed in previous studies (e.g., Killworth and Hughes 2002; Firing et al. 2011; Klocker et al. 2012b). The horizontal structure of eddy velocity magnitude is consistent with that observed in altimetry (e.g., Farneti et al. 2010): eddy velocity magnitudes are large along the path of the ACC and are also larger to the east of Drake Passage than to the west. Second, as reviewed in section 1, in the spectra of sea surface height from altimetry, both westward- and eastward-propagating signals are significant in the Southern Ocean and Kuroshio Extension patches, where the eastward mean flow is intense (Wortham 2013). Similar features exist in the POP model (Fig. 3). Note that the model resolution is high enough to be eddy permitting. In this area of the model, the domain average of the first baroclinic Rossby radius of deformation R_d is 12 km, which is twice as large as the POP grid spacing averaged over the study domain. Additionally, R_d is larger than the grid size at 88% of grid points in our study domain.
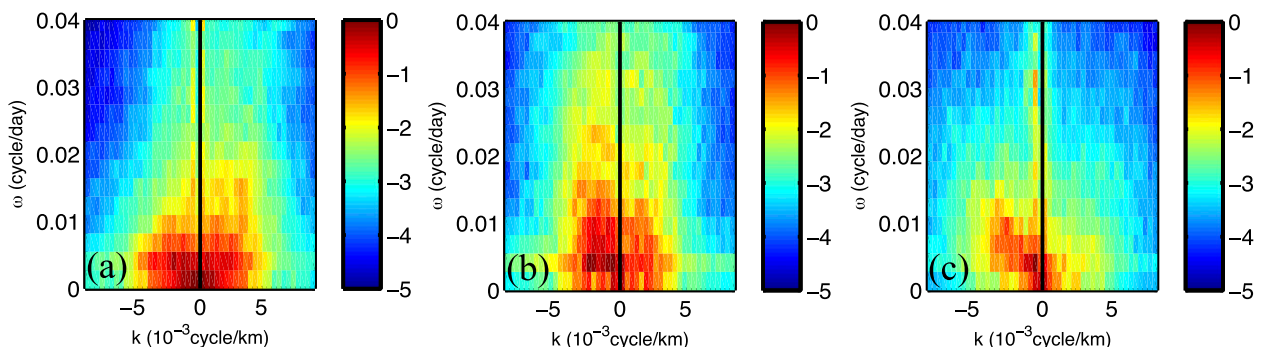

FIG. 3. Base 10 logarithm of the normalized frequency–zonal wavenumber spectrum of sea surface height in a patch extending over 30° longitude and 10° latitude from (a) the Southern Ocean, (b) the Kuroshio Extension, and (c) the interior of the North Pacific. The center locations of the patches are 40°S, 15°W for (a), 35°N, 160°E for (b), and 30°N, 140°W for (c). The spectra were obtained from the sea surface height from the POP model during 1997/98, with the spatial and temporal mean over each patch removed. Black lines indicate the zero zonal wavenumber and thus separate eastward- and westward-propagating signals in the spectra.

4. Eddy diffusivities in the DIMES region from numerical floats

a. Methodology

Chen et al. (2014) calculated critical layer depths and float-based eddy diffusivities in the Kuroshio Extension. This study uses a similar approach to estimate diffusivities from floats. As in Griesel et al. (2010) and Chen et al. (2014), we diagnose cross-stream diffusivities using Eq. (18). Residual velocities $u'_{\perp,L}$ represent the deviation of the float velocities from the local time-mean Eulerian velocities at the float positions. Here, the time mean refers to the temporal average over the years 1994–95. We gather positions of floats within our study domain every other day; these serve as the center positions of the pseudotrajectories. Float trajectories that extend 69 days backward in time and 69 days forward in time relative to the center position are used in the analysis (Chen et al. 2014).

We use a clustering approach, described by Chen et al. (2014), to divide our domain into adaptive bins. These bins are irregularly distributed in space; however, the number of pseudotrajectories in each bin is roughly the same (Fig. 4). This statistical uniformity leads to more converged diffusivity estimates than the geographic binning approach (Koszalka and LaCasce 2010; Chen et al. 2014). We estimated diffusivities in these adaptive bins at 11 depth intervals in the upper 3000 m with layer thicknesses increasing from 45 to 500 m with depth. Using the Chen et al. (2014) technique to test for convergence, we found that diffusivity estimates in 95% of the adaptive bins were converged.

b. Numerical results

The horizontal patterns of float-based cross-stream diffusivities, as shown in Fig. 5, are similar to those of the eddy velocity magnitudes shown in Fig. 2, with large values inside the ACC. This indicates that the spatial patterns of eddy mixing are probably mostly controlled
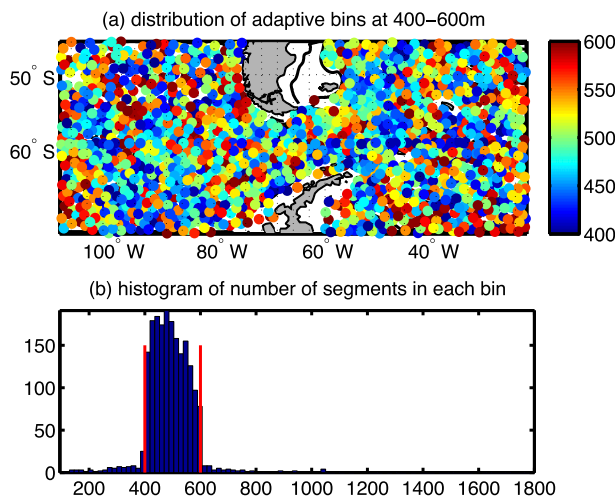

FIG. 4. (a) Colored dots indicate the location of centroids for each adaptive bin for diffusivity estimates at 400–600 m. The color of the dots shows the number of pseudo tracks for each bin. (b) Histogram of the number of tracks per bin and red lines indicate the location of the numbers 400 and 600. The number of pseudo tracks for each bin is around 500, and the length of each pseudo track is 139 days.

by eddy kinetic energy. Similar to the eddy velocity magnitude (Fig. 2), the horizontal structures of eddy diffusivities change little with depth, consistent with the equivalent barotropic nature of the flow field in the Southern Ocean. Diffusivities in the ACC east of the Drake Passage are larger than those to the west. Negative float-based diffusivities exist at some spots, especially inside the ACC (Fig. 5). They correspond to upgradient eddy fluxes, which have been identified in many oceanic regions from both observations and modeling studies (e.g., Johnson et al. 1992; Morrow et al. 1992; Wilkin and Morrow 1994; Griesel et al. 2009; Chen et al. 2014).

The vertical structures of float-based diffusivities and mixing lengths from the POP model were examined by Griesel et al. (2014). They found that the mixing
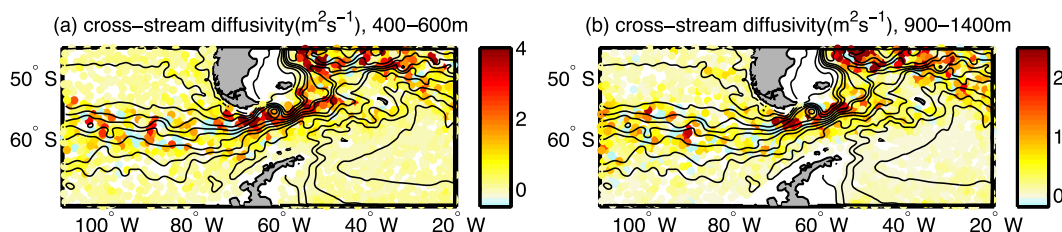

FIG. 5. Float-based diffusivities in the cross-stream direction at (a) 400–600 and (b) 900–1400 m. Dots indicate the location of the centroid of each adaptive bin used to obtain the diffusivity estimates. We carried out convergence tests using the method from Chen et al. (2014) and only converged diffusivities are shown here. Black lines indicate the barotropic streamlines. Gray regions denote land, and white regions denote areas lacking converged diffusivity estimates due to topography or inadequate numbers of floats.
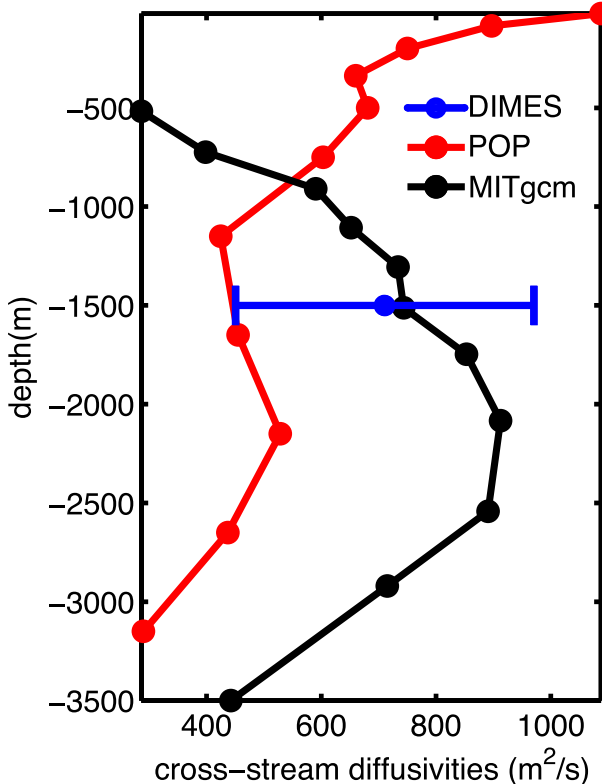
FIG. 6. The figure compares diffusivities from Fig. 10 in Tulloch et al. (2014) (blue dot and error bar and black line) with those from this study (red line). The blue dot and error bar show meridional eddy diffusivities observed from the DIMES experiment, and the black line shows the meridional eddy diffusivities estimated using numerical tracers from the MITgcm. The red line shows the float-based cross-stream diffusivities in the POP model averaged over a selected region west of the Drake Passage (61°–56°S, 110°–80°W). This region approximately coincides with that of the spreading area of the numerical tracers used in Tulloch et al. (2014) one year after their release [see Fig. 1b from Tulloch et al. (2014)]. Therefore, the red and black lines represent diffusivities in the same area.

suppression in the jet core is not robust east of the Drake Passage, where the mean flow is composed of multiple thin jets. We repeated their analysis, and our findings support their conclusions (not shown).

LaCasce et al. (2014) and Tulloch et al. (2014) estimated meridional isopycnal diffusivities, using tracer and float observations collected during the DIMES experiment. Given the quasi-zonal orientation of the ACC west of the Drake Passage, their meridional diffusivities are expected to be approximately equivalent to cross-stream diffusivities. They extrapolated the vertical structures of the meridional diffusivities from the DIMES observations using a regional eddying model. However, their estimates do not resolve horizontal structures.

Figure 6 shows a comparison of our float-based diffusivities in a region west of the Drake Passage

(61°–56°S, 110°–80°W) with those from a regional MITgcm simulation (Tulloch et al. 2014). Estimates from Tulloch et al. (2014) and our modeling results agree both in the order of magnitude of the diffusivities and the location of the deep maximum. Below 1000 m, the vertical structure of our diffusivity profile is similar to that of Tulloch et al. (2014), with both displaying peak values at around 2100 m; our estimate, however, is of a smaller magnitude (Fig. 6). At 500–1000 m, our float-based diffusivities decrease with depth, but theirs increase with depth. These diffusivity differences might be due to their model having higher horizontal and vertical resolution than ours. Also, their estimates are based on 12 patches of tracers, whereas ours are based on numerical floats deployed at high spatial resolution. Note, however, that the observational estimate from DIMES at 1500 m (the blue error bar in Fig. 6) encompasses our estimate, although our float-based diffusivity estimates are for the year 1994, roughly 15 yr prior to the initial DIMES float and tracer deployment (e.g., Ledwell et al. 2011).

5. Eddy diffusivities in the DIMES region from multiwavenumber theory: Estimations and comparisons

This section examines diffusivities and mixing lengths from the MW theory from section 2 and compares them with those from the F–N theory and from numerical floats.

a. Methodology

To assess whether we can obtain improved mixing estimates by extending the single-wavenumber theory to the multiwavenumber scenario, we diagnose eddy diffusivities and mixing lengths from both the F–N and MW theories. In contrast to Tulloch et al. (2014), we consider the entire DIMES domain, both upstream and downstream of Drake Passage.

We use $\kappa_\perp^{\text{multi}}$ to denote the cross-stream diffusivities from the multiwavenumber mixing formula Eq. (20) and $L_{\text{mix},\perp}^{\text{multi}}$ for the corresponding mixing lengths. Similarly, $\kappa_\perp^{\text{single}}$ and $L_{\text{mix},\perp}^{\text{single}}$ respectively denote cross-stream diffusivities and mixing lengths from the F–N theory.

The diffusivity $\kappa_\perp^{\text{multi}}$ depends on the frequency–wavenumber spectrum of cross-stream eddy velocities $S_{u'_\perp, u'_\perp}(k', \omega', \mathbf{x})$. As illustrated in Fig. 7c, we identify a 300-km-long slice (black line in Fig. 7c), which is centered at the position $\mathbf{x}$ (red dot in Fig. 7c) and aligned with the mean flow direction at the position $\mathbf{x}$. Then we extract Eulerian eddy velocities along the slice during the year 1994 to form the Hovmöller diagram [Figs. 7a(1) and 7b(1)]. The term $S_{u'_\perp, u'_\perp}$ can be obtained from the extracted
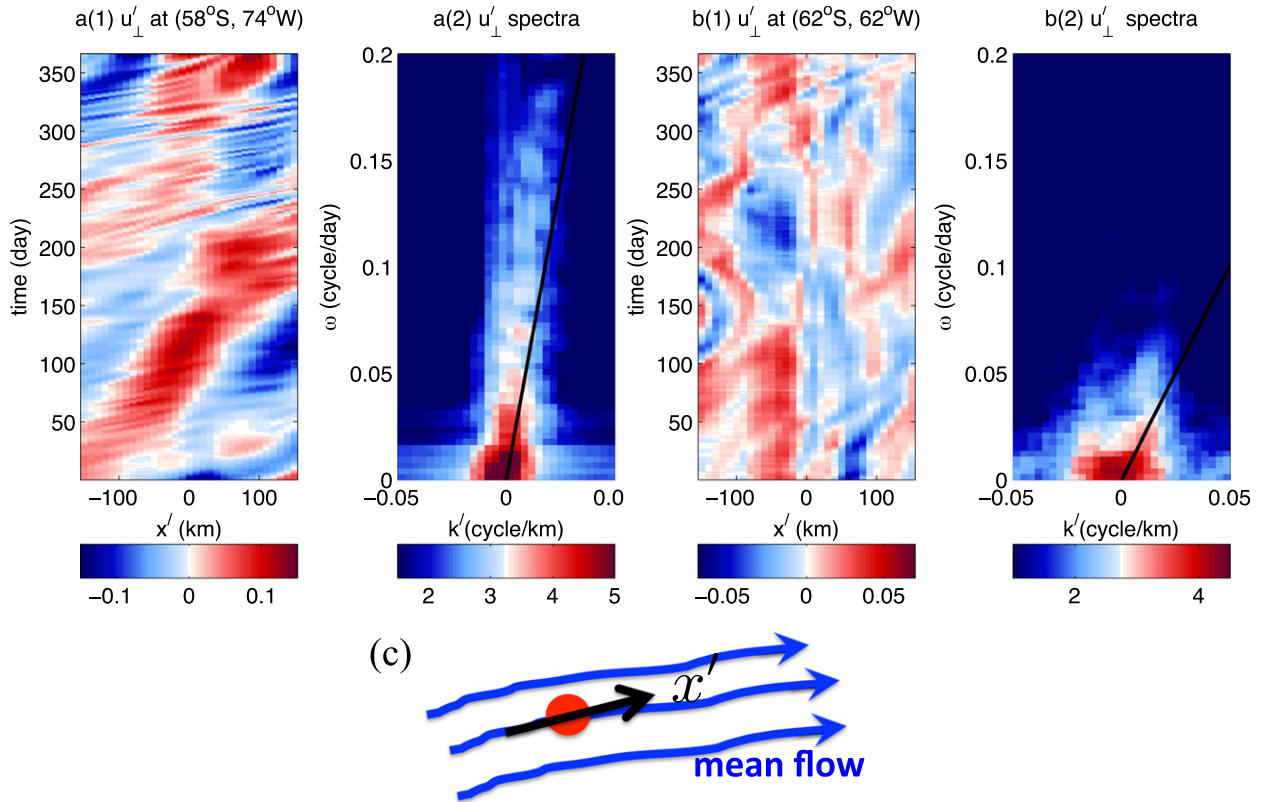
FIG. 7. [a(1)] Hovmöller diagram of cross-stream velocity anomalies (m s^{-1}) along the mean flow direction x', extending from -150 to 150 km at 918 m in the year 1994. Here $x' = 0$ [i.e., red dot in (c)] corresponds to 58°S, 74°W. (c) As in Fig. 8b in Chen et al. (2014), to form a Hovmöller diagram centered at the red dot, we first identify a 300-km slice (the black line), which is centered at the red dot and aligns with the mean flow direction at the red dot. Cross-stream velocity anomalies along the black line are then extracted to form the Hovmöller diagram. Cross-stream velocity anomalies denote the deviation of velocities in the cross-mean flow direction from its mean over the years 1994–95. [b(1)] As in [a(1)], but for a different location: 918 m at 62°S, 62°W. [a(2)], [b(2)] Frequency–wavenumber spectra of velocity anomalies shown in [a(1)] and [b(1)], respectively. Black lines in [a(2)] and [b(2)] denote $\omega = |\mathbf{U}|k'$, where $|\mathbf{U}|$ is the mean flow magnitude, ω denotes frequency, k' is the wavenumber along the x' direction, and positive k' points in the mean flow direction. The color bars of the spectra are on the logarithmic scale, and the unit of the spectra is m^2 s^{-2} (cpk)$^{-1}$ (cpd)$^{-1}$, where cpk denotes cycle per km and cpd denotes cycle per day.

eddy velocities using a two-dimensional Fourier transform [Figs. 7a(2) and 7b(2)]. We then determine $\kappa_\perp^{\text{multi}}$ by integrating $S_{u'_\perp,u'_\perp}$ along $\omega' = |\mathbf{U}|k'$ [Eq. (20)].

We diagnose $L_{\text{mix},\perp}^{\text{single}}$ from the F–N theory [Eq. (2)], using the same method as Chen et al. (2014). The dominant eddy wavenumber k_{eddy} is chosen to be the centroid of the eddy kinetic energy spectrum. The eddy size and the reciprocal of the eddy decorrelation time scale are determined from

$$L(x,y,z) = \frac{2\pi}{k_{\text{eddy}}(x,y,z)}, \quad \text{and} \quad \gamma(x,y,z) = \frac{u_{\text{rms}}(x,y,z)}{2\Gamma L(x,y,z)}.$$
(23)

As before, u_{rms} is the eddy velocity magnitude, and Γ denotes the mixing efficiency. We chose Γ to be 0.35, following Klocker and Abernathey (2014) and Chen

et al. (2014). The phase speed C_w is determined from the Radon transform approach of Chen et al. (2014), and $\mathbf{U}$ denotes the 2-yr (1994/95) mean flow vector. We can then determine $\kappa_\perp^{\text{single}}$ from the mixing length $L_{\text{mix},\perp}^{\text{single}}$ using Eq. (1):

$$\kappa_\perp^{\text{single}}(x,y,z) = \Gamma u_{\text{rms}}(x,y,z) L_{\text{mix},\perp}^{\text{single}}.$$
(24)

Similarly, $L_{\text{mix},\perp}^{\text{multi}}$ can also be obtained from $\kappa_\perp^{\text{multi}}$ using Eq. (1).

b. Results

1) COMPARISON OF HORIZONTAL STRUCTURES

Figure 8 shows cross-stream diffusivities from the two theories and numerical floats. Consistent with float-based results, both the MW and F–N theories represent
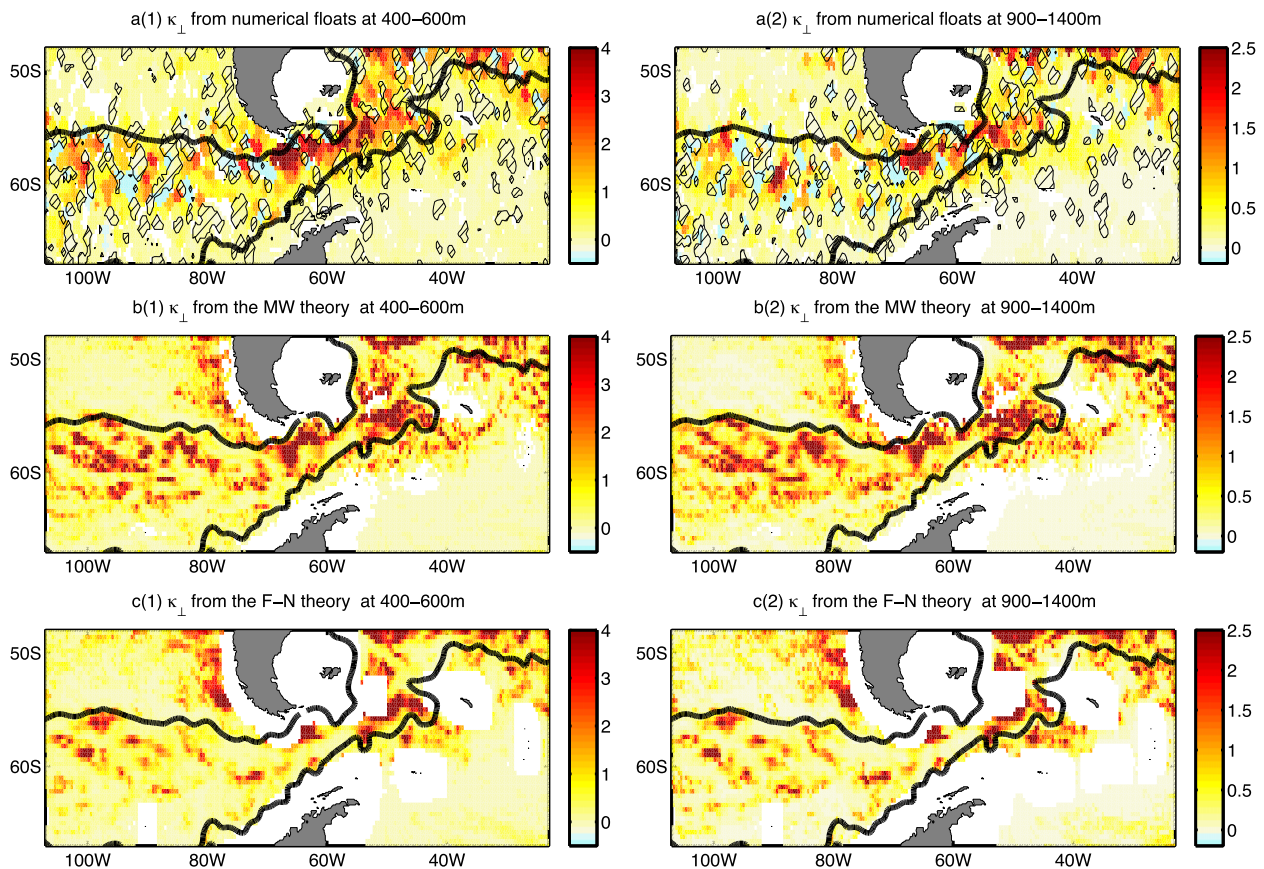
FIG. 8. Cross-stream eddy diffusivities ($10^3 \, \mathrm{m^2 \, s^{-1}}$) from [a(1)],[a(2)] numerical floats, [b(1)],[b(2)] the MW theory, and [c(1)],[c(2)] the F–N theory at (left) 400–600 and (right) 900–1400 m. The two thick black contours are the barotropic streamlines with values of 3×10^4 and $10^5 \, \mathrm{m^2 \, s^{-1}}$, which approximately pass the northern and southern edges of the Drake Passage. They are chosen to be the boundaries of the ACC. The hatched area indicates regions where diffusivities are indistinguishable from zero at the 95% confidence level (i.e., the magnitude of diffusivity is smaller than the two standard error using a bootstrap technique). Gray regions denote land, and white regions denote areas lacking diffusivity estimates due to topography or inadequate numbers of floats. Note that the white area in [c(1)] and [c(2)] is larger than in [b(1)] and [b(2)], as the eddy size L at each grid point used to estimate $\kappa_\perp^{\mathrm{single}}$ from the F–N theory is derived from flow properties from a $3° \times 3°$ patch (Chen et al. 2014), while $\kappa_\perp$ from the MW theory at each grid point is derived from a 300-km slice (section 5a).

large diffusivities occurring inside the ACC. However, both theories have large diffusivity estimates along the eastern coast of the South Pacific, which is not the case for the float-based estimates. Possible reasons for this overestimation are discussed in section 5b(3). Float-based diffusivities are negative at some spots, corresponding to upgradient eddy fluxes. However, neither the F–N nor MW theories can represent negative diffusivities, whose mechanism and parameterization are left for future work.

Cross-stream mixing lengths have complex horizontal patterns (Fig. 9). The MW theory reasonably represents the large mixing lengths inside the ACC below 1000 m, but the F–N theory does not (right panel of Fig. 9). Both the MW and F–N theories fail to capture effectively the large-scale structures of mixing lengths in the upper 1000 m (left panel of Fig. 9). In particular, the mixing

length from the F–N theory is too large north of the ACC west of the Drake Passage because of the large eddy sizes L.

To quantify the skill of the two theories in representing diffusivities, we correlated the float-based estimates with those diagnosed using the MW and F–N theories (Fig. 10). Both theories capture some aspects of the horizontal structure of cross-stream diffusivities; the correlation coefficients between the float-based estimates and the MW theory estimates have roughly the same magnitude as those between floats and the F–N theory, with values of 0.4–0.6 (Fig. 10b). The similar skill of the two theories in capturing cross-stream diffusivity patterns is related to the fact that, in our study domain, the diffusivity patterns are mainly controlled by eddy kinetic energy. This indicates that obtaining accurate mixing lengths (e.g., Bates et al. 2014; Chen et al. 2014)
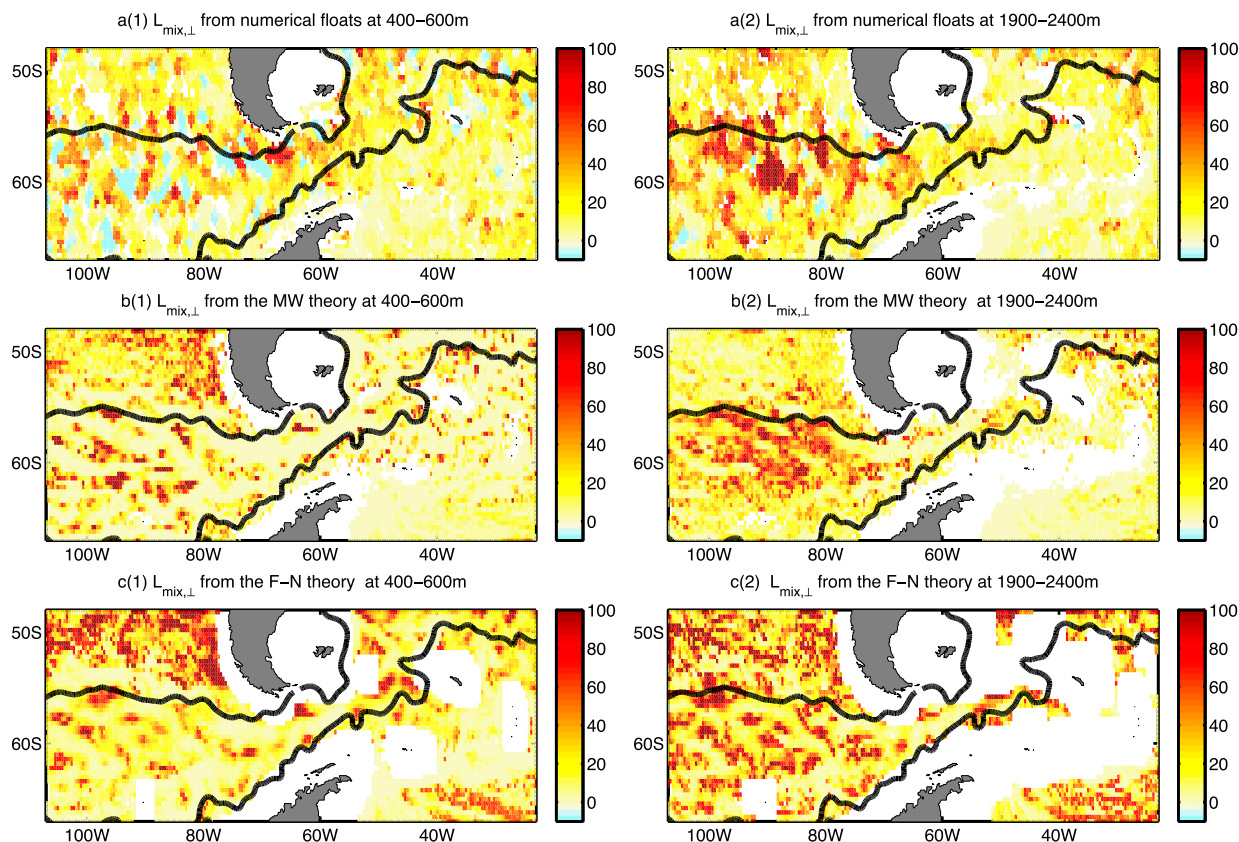
FIG. 9. Cross-stream mixing lengths ($L_{\mathrm{mix},\perp}$; km) from [a(1)],[a(2)] numerical floats, [b(1)],[b(2)] the MW theory, and [c(1)],[c(2)] the F–N theory at (left) 400–600 and (right) 1900–2400 m. As in Fig. 8, the two thick black contours represent the boundaries of the ACC. Gray regions denote land, and white regions denote areas lacking diffusivity estimates due to topography or inadequate numbers of floats.

may not be essential to obtaining the correct diffusivity structures in the DIMES region.

When we examine the horizontal structures of cross-stream mixing lengths below 500 m, we see that the correlation coefficients between the MW theory and floats are larger than those between the F–N theory and floats (Fig. 10a). The advantage of the MW theory is more noticeable with increasing depth. Below 2000 m, mixing lengths diagnosed from the F–N theory and float-based estimates decorrelate, whereas the correlation coefficient between the MW theory estimates and float-based estimates increases to 0.3–0.4 (Fig. 10a).

2) COMPARISON OF VERTICAL STRUCTURES

To assess how well the two theories capture the vertical structures of eddy mixing, we examined the correlation between float-based diffusivities/mixing lengths and their theoretical-based counterparts throughout the water column (Fig. 11). In the regions where correlation coefficients are not significantly positive, the theory is considered not to have skill in representing diffusivities. Larger positive correlation coefficients imply better skill

in representing diffusivities. Table 1 quantitatively compares the skill of the two theories.

The F–N theory has better skill representing diffusivities inside the ACC than outside the ACC [Figs. 11b(1) and 11b(2)]; it captures the vertical structures of the cross-stream diffusivities in 75% of the area inside of the ACC but in only 41% of the area outside of the ACC (Table 1). For vertical structures of cross-stream mixing lengths, the F–N theory provides skillful estimation in 55% of the area inside the ACC but only 19% of the area outside the ACC (Table 1).

The MW theory better represents the vertical structures of diffusivities and mixing lengths than the F–N theory both inside and outside the ACC (Fig. 11; Table 1). In 91% of the study domain, the MW theory represents vertical structures of diffusivities that are significantly correlated with float diffusivities. In contrast, the percentage is only 55% for the F–N theory. Table 1 reveals that the MW theory captures diffusivities outside the ACC as well as it does inside the ACC. In contrast, the F–N theory is better inside the ACC than outside. Nonetheless, the MW theory consistently outperforms
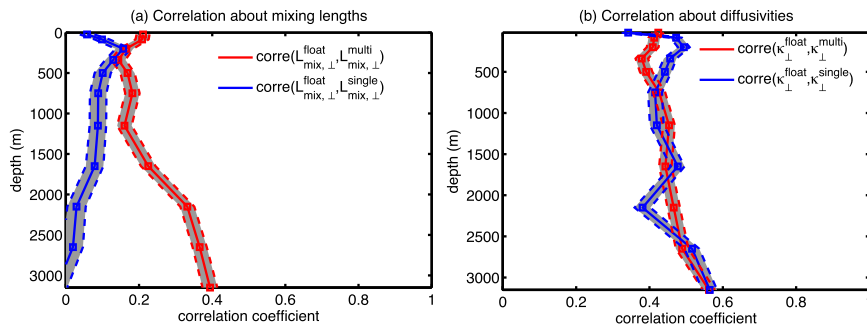
FIG. 10. Correlation of (a) cross-stream mixing lengths and (b) diffusivities as a function of depth. In the legends, $L_{\text{mix},\perp}$ and $\kappa_\perp$ respectively denote mixing length and diffusivities in the cross-stream direction. Superscripts float, multi, and single denote estimates from floats, the MW theory, and the F–N theory, respectively.

the F–N theory. Overall, in roughly 90% of the area outside the ACC, the float-based estimates are better correlated with estimates from the MW theory, than with estimates from the F–N theory (Table 1). In contrast, the percentage is roughly 60% inside the ACC.

The MW theory better represents the mixing lengths to the east of the Drake Passage than to the west [Fig. 11a(2)]. The MW theory cannot represent negative diffusivities. The existence of negative diffusivities inside the ACC west of the Drake Passage (Figs. 8, 9) probably contributes to the small or negative correlation there. Note that the MW theory is based on the

assumptions that the mean flow varies slowly spatially and that eddies have much smaller amplitude than the mean flow. These assumptions are poorly satisfied in the area north of the ACC west of the Drake Passage (not shown), leading to the poor representation of mixing lengths there [Fig. 11a(2)].

3) COMPARISON OF MAGNITUDES

Though the MW and F–N theories capture the order of magnitude of eddy diffusivities and mixing lengths correctly, both theories overestimate the values (Fig. 12). In the upper 1000 m, the MW theory overestimates the
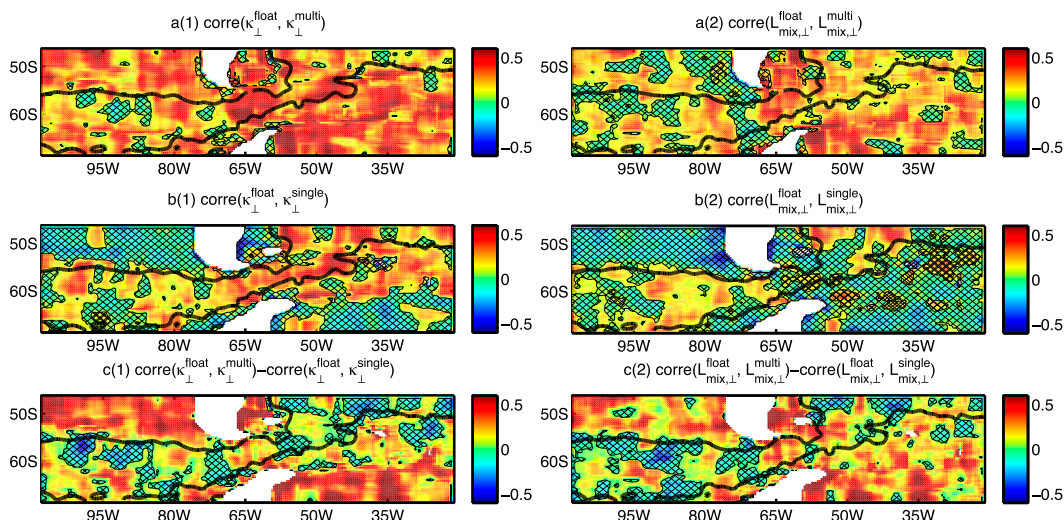

FIG. 11. Correlation of float-based mixing quantities vs MW and F–N counterparts. In the title of each panel, (left) $\kappa_\perp$ and (right) $L_{\text{mix},\perp}$ denote diffusivities and mixing lengths in the cross-stream direction, respectively; corre(α, β) is defined as the correlation between variables α and β over a $3.2° \times 3.2°$ patch that extends from surface to bottom; superscripts float, multi, and single, respectively, indicate estimates from numerical floats, MW theory, and F–N theory. [a(1)],[a(2)],[b(1)],[b(2)] Regions where correlation coefficients are not significantly positive at 95% confidence level are hatched; [c(1)],[c(2)] regions with negative values are hatched. As in Fig. 8, the region inside the two black contours is defined to be inside the ACC; the rest of the area in our study domain is defined to be outside the ACC.

TABLE 1. Percentage of the area that satisfies the criteria listed in the first column at 95% confidence level, in the entire domain, inside the ACC and outside the ACC. Here, we define corre(α, β) as the correlation between variables α and β in the entire water column over a $3.2° \times 3.2°$ patch. Superscripts float, multi, and single, respectively, indicate estimates in the cross-stream direction from numerical floats, MW theory, and F–N theory. The terms $\kappa_\perp$ and $L_{\text{mix},\perp}$, respectively, denote eddy diffusivities and mixing lengths in the cross-stream direction. The two thick black contours of the barotropic streamlines in Fig. 8, with the value of 3×10^4 and 10^5 m^2 s^{-1}, approximately pass the northern and southern edges of the Drake Passage. They are chosen to be the boundaries of the ACC, the region inside the two black contours is defined to be inside the ACC, and the rest of the area in our study domain is defined to be outside the ACC. Reported uncertainties here are two standard errors, obtained from 10 realizations of a bootstrapping technique by randomly sampling the gridded values in the selected spatial domain.

Region	Entire domain (%)	Inside ACC (%)	Outside ACC (%)
corre($\kappa_\perp^{\text{float}}, \kappa_\perp^{\text{multi}}$) > 0	91 ± 1	86 ± 1	95 ± 1
corre($\kappa_\perp^{\text{float}}, \kappa_\perp^{\text{single}}$) > 0	55 ± 1	75 ± 1	41 ± 1
corre($\kappa_\perp^{\text{float}}, \kappa_\perp^{\text{multi}}$) $-$ corre($\kappa_\perp^{\text{float}}, \kappa_\perp^{\text{single}}$) > 0	77 ± 1	62 ± 2	87 ± 1
corre($L_{\text{mix},\perp}^{\text{float}}, L_{\text{mix},\perp}^{\text{multi}}$) > 0	73 ± 0	72 ± 1	74 ± 1
corre($L_{\text{mix},\perp}^{\text{float}}, L_{\text{mix},\perp}^{\text{single}}$) > 0	34 ± 1	55 ± 1	19 ± 1
corre($L_{\text{mix},\perp}^{\text{float}}, L_{\text{mix},\perp}^{\text{multi}}$) $-$ corre($L_{\text{mix},\perp}^{\text{float}}, L_{\text{mix},\perp}^{\text{single}}$) > 0	77 ± 1	60 ± 1	88 ± 1

domain-averaged diffusivities and mixing lengths more than the F–N theory; below 1000 m, the mismatch between the MW theory and floats is smaller than it is between the F–N theory and floats.

The magnitude of the diffusivities from the F–N theory depends on the choice of Γ, which denotes the mixing efficiency. The parameter Γ is generally chosen to be order one (e.g., Klocker and Abernathey 2014; Chen et al. 2014). We examined the diffusivities from the F–N theory using different choices of Γ. F–N theory's overestimation of diffusivities between 85 and 3000 m is insensitive to Γ within the wide range from 0.1 to 10.

Since both the F–N and MW theories overestimate diffusivities, in particular, along the eastern coast of the South Pacific (Figs. 8, 12), the single-wavenumber assumption probably is not the leading-order explanation for the overestimation. When diagnosing the float-based diffusivities, in order to reduce the dispersion caused by the mean flow shear, as Griesel et al. (2010) did, we calculate residual velocities from Eq. (18) by subtracting the local mean flow rather than the spatially uniform mean flow. However, both the F–N and MW theories assume the mean flow to be constant and thus do not include a mechanism to reduce the dispersion due to mean flow shear. Therefore, the spatial homogeneity assumption inherent in these theories might contribute to the overestimation.

To test this hypothesis, we use Eq. (18) to recalculate the float-based cross-stream diffusivities $\kappa_{\perp,\text{sheared}}$ by assuming that the mean flow is constant along each float trajectory and equal to the mean flow at the midpoint of the trajectory, that is, at the position where the float passes at time t_0. In other words, the residual velocity is defined as the deviation of eddy velocity along the float trajectories from the mean flow at the float position at

time t_0. Similar to the F–N and MW theories, the constant mean flow calculation does not include a mechanism to reduce the dispersion caused by the mean flow shear. As we expected, similar to the theory-based diffusivities, the domain-averaged $\kappa_{\perp,\text{sheared}}$ is also larger than our original float-based estimates, and $\kappa_{\perp,\text{sheared}}$ also overestimate values off the east coast of South America (figure not shown).

6. Discussion

The main goal of the MW theory was to modify the single-wavenumber theory to account for the multi-wavenumber feature of eddies. The single-wavenumber theory and the MW theory are consistent in some respects. In the single-wavenumber limit, the MW theory reduces to the single-wavenumber mixing formula of Ferrari and Nikurashin (2010) (appendix A). In addition, both theories are based on an assumption of spatial homogeneity, which means that horizontal variations in the mean flow and eddy properties are negligible. Finally, both theories explicitly illustrate the effect of the mean flow **U** on mixing.

In spite of their consistency, the single-wavenumber and MW theories also have clear differences. The MW theory more clearly depicts the ocean, in that oceanic eddies are composed of a range of wavenumbers rather than a single dominant wavenumber. In addition, the MW theory provides formulas for the diffusivity tensor and cross-stream diffusivities [Eqs. (17) and (20)]; in contrast, the F–N theory only focuses on cross-stream diffusivities.

Since the MW theory is in spectral form, it can be used to estimate the mixing rates induced by eddies at selected spatiotemporal scales. Separating the
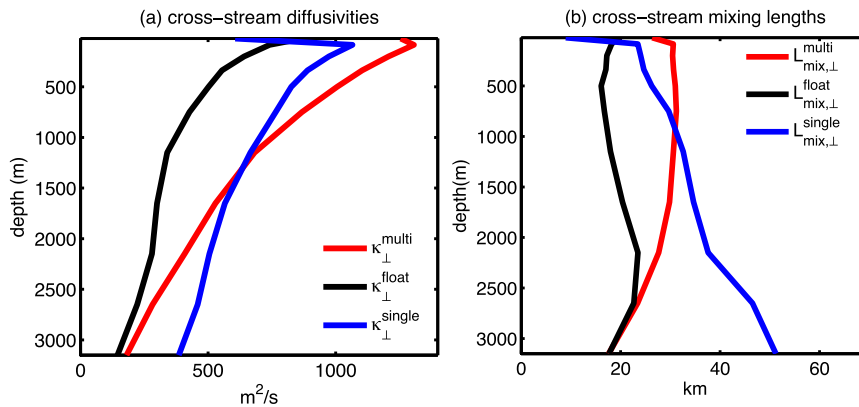
FIG. 12. The domain averaged (a) cross-stream diffusivities and (b) mixing lengths as a function of depth from the MW theory (red), numerical floats (black), and from the F–N theory (blue).

contributions of small-scale and large-scale eddies to mixing is useful because in eddy-permitting models, large eddies are explicitly resolved and only small eddies need to be parameterized (e.g., Fox-Kemper and Menemenlis 2008). Separating the contributions of low-frequency and high-frequency eddies to mixing is also useful because in contrast with high-frequency eddies, low-frequency eddies are dominated by banded structures (striations) leading to anisotropic mixing (e.g., Maximenko et al. 2005; Chen et al. 2015). The MW theory [Eq. (20)] tells us that the contribution to cross-stream mixing from eddies with frequencies lower than Ω_S is

$$\kappa_{\perp}^{\text{multi}}(\mathbf{x}) \text{ from striations}$$
$$= \frac{1}{2} \int_{-\Omega_S/|\mathbf{U}|}^{+\Omega_S/|\mathbf{U}|} S_{u'_{\perp} u'_{\perp}}(k', |\mathbf{U}|k', \mathbf{x}) \, dk'. \quad (25)$$

The advantage of Eq. (25) is that it is computationally more efficient than some other related frameworks (e.g., Chen 2013; Chen and Flierl 2015).

Our work regarding the MW theory has several implications. First, the fact that the MW theory outperforms the F–N theory in capturing the mixing length structures indicates that it is useful to consider the multiwavenumber regime in future development of mixing theories and eddy parameterizations. In addition, much effort has been devoted to characterizing and interpreting oceanic spectra in order to reveal the underlying processes of oceanic turbulence (e.g., Xu and Fu 2011). The MW theory links velocity spectra with mixing, underscoring the importance of spectra for mixing. Finally, critical layer theory suggests that elevated values of mixing lengths occur at the critical layer depth, where the wave phase speed matches the mean

flow magnitude (e.g., Bretherton 1966; Green 1970). Critical layer depth has been estimated either by identifying the phase speed of the fastest growing mode from linear stability analysis (e.g., Smith and Marshall 2009) or by identifying the dominant phase speed of the eddy field through the Radon transform (Chen et al. 2014). Each wavenumber in the eddy field corresponds to a different critical layer depth, and this work indicates that it is important to consider the contribution of all the waves in the eddy field to mixing. Therefore, future studies would potentially benefit from estimating a critical layer depth specific to each wavenumber.

Though successful in many respects (as shown in Fig. 12), the MW theory, like the F–N theory, overestimates the domain-averaged cross-stream mixing lengths by roughly 5–10 km. As discussed in section 5b(3), the spatial homogeneity assumption inherent in these theories contributes to the overestimation. Further improvements to the mixing theory probably should take into account the spatial inhomogeneity (e.g., horizontal shear in the mean flow), which can be induced by topographic effects, the localized formation of coherent vortices, and so on. In addition, both the MW and F–N theories are built on the assumption that the magnitudes of eddies are smaller than that of the mean flow. This linear assumption does not hold in many oceanic regions, and taking this nonlinearity into account may lead to improvements of the mixing theory.

It is not trivial to take into account the spatial inhomogeneity in eddy parameterizations. Appendix B illustrates analytically that, in an inhomogeneous system, where the mean tracer gradient and eddy fluxes vary over short spatial scales, eddy mixing depends on both the local and nonlocal mean tracer gradients. However, the concept of the eddy diffusivity itself, on which the F–N and MW theories are built, is based on the assumption

that eddy mixing and transport processes can be parameterized using the local mean tracer gradient.

While the shortcomings of the MW theory identified in this study indicate that nonlocal eddy parameterization schemes may ultimately prove valuable, the MW theory nonetheless merits further assessment, particularly since the assumption of spatial homogeneity is reasonable in regions such as the midlatitude ocean interior. In addition to cross-stream diffusivities, the MW theory also provides formulas for the diffusivity tensor. The relevance of the MW theory to mixing in other regions or other years has not yet been explored. Griesel et al. (2015, manuscript submitted to *Ocean Modell.*) diagnosed the diffusivities from the single-wavenumber theory using eddy parameters obtained from linear instability analysis and then compared them with those from numerical floats in the entire Southern Ocean. While they found evidence for enhanced Lagrangian integral time scales at the steering level depth, they concluded that a single frequency is not able to reproduce the oscillations in the velocity autocovariance. This suggests that it would be useful to assess whether the MW theory also better captures the vertical structure of mixing outside of the DIMES region.

To infer eddy diffusivities from the single-wavenumber and multiwavenumber theories, we need information about eddies (e.g., their spectra and dominant phase speed). Thus, these mixing theories are not directly applicable to eddy parameterization schemes, which are intended to link eddy diffusivities with large-scale, mean flow characteristics. However, the theories do underscore the value of including the critical-layer effect in eddy parameterization schemes, and the multiwavenumber theory shows that the critical-layer depth is wavenumber specific. The multiwavenumber theory also suggests that the link between the large-scale mean flow and eddy spectra may help formulate new eddy parameterization schemes. Previous studies linking mean flow with eddy properties exist (e.g., Venaille et al. 2011).

7. Summary

Though oceanic eddies contain motions spanning a wide range of wavenumbers (e.g., Wunsch 2010), previous theories of eddy mixing have often been based on the assumption that eddies are composed of a single or dominant wave (e.g., Green 1970; Killworth 1997; Ferrari and Nikurashin 2010; Klocker et al. 2012a). Motivated by this discrepancy, we formulated a MW theory of mixing, starting from the problem described by Klocker et al. (2012a). Our MW theory, which can be derived from both Lagrangian and Eulerian perspectives, is based only on the mean flow and eddy velocity

spectra, which are unambiguous and straightforward to calculate.

We chose the DIMES region to compare mixing theories. Eddy diffusivities and mixing lengths in the cross-stream direction were estimated using numerical floats deployed in a global eddying model. Cross-stream diffusivities are large inside the ACC, where eddy amplitudes are large. Horizontal structures of cross-stream diffusivities and eddy kinetic energy vary little with depth, indicating the relevance of the equivalent barotropic nature in this region. These float-based mixing estimates at high spatial resolution can serve as a context for observational results from the DIMES experiment.

The float-based mixing estimates were then compared with those from both the F–N and MW theories. We found that the F–N and MW theories have similar skill in representing the horizontal structures of cross-stream eddy diffusivities, which are mainly controlled by eddy velocity magnitudes. Correlation analysis indicates that, compared to the F–N theory, the MW theory is better at capturing both the horizontal and vertical structures of cross-stream mixing lengths. Therefore, a so-called dominant wave is insufficient to capture the mixing length properties in the DIMES area and possibly in other ocean regions as well. Ideally the full range of waves in the ocean should be considered when developing new mixing theories or parameterization schemes.

APPENDIX A

Consistency between the Single- and Multiwavenumber Theories in the Single-Wavenumber Scenario

Here, we illustrate that, in the single-wavenumber scenario, the cross-stream diffusivity from the MW theory in

section 2 is consistent with the single-wavenumber formula for cross-stream diffusivities from Ferrari and Nikurashin (2010) (F–N theory).

a. Review of the F–N theory

Following Flierl and McGillicuddy (2002), Ferrari and Nikurashin (2010) assumed that eddies are forced by stochastic time-varying forcing with a single wavenumber. They employed a surface quasigeostrophic model and defined the mean velocity U and buoyancy B as

$$U(z) = U_0 \frac{z + H}{H}, \quad \text{and} \quad B(y,z) = -\Gamma y + N^2 z, \quad (A1)$$

where N is the buoyancy frequency; $\Gamma = fU_0/H$, denoting the horizontal buoyancy gradient; and f is the Coriolis parameter. The eddy field satisfies

$$\frac{\partial}{\partial t} b + U_0 \frac{\partial}{\partial x} b - \Gamma \frac{\partial}{\partial x} \psi = \mathbb{U}\sqrt{\gamma} \, \text{Re}[r(t)e^{i(kx+ly)}] - \gamma b,$$
$$z = 0, \quad (A2)$$

and

$$\partial_x^2 \psi + \partial_y^2 \psi + \frac{f^2}{N^2}\partial_z^2 \psi = 0, \quad z < 0, \quad (A3)$$

where ψ is eddy streamfunction, b is surface eddy buoyancy, k is the zonal wavenumber, l is the meridional wavenumber, γ is the linear damping rate, and $r(t)$ is the white noise forcing with zero mean and autocorrelation function $\langle r(t)r^*(t')\rangle = \delta(t - t')$. The term $\mathbb{U}$ sets the forcing and eddy amplitudes.

Solutions satisfying Eqs. (A2) and (A3) can be written as

$$\psi(x,y,z,t) = \frac{\mathbb{U}}{\kappa} \text{Re}\left\{ a(t) \exp\left[i(kx + ly) + \frac{N\kappa}{f}z \right] \right\}, \quad \text{and}$$
$$b(x,y,z,t) = N\kappa\psi(x,y,z,t), \quad (A4)$$

where κ is the wavenumber magnitude $\sqrt{k^2 + l^2}$. Substituting Eq. (A4) into Eq. (A2) gives

$$\frac{da}{dt} + \left[\gamma + ik\left(U_0 - \frac{\Gamma}{N\kappa} \right) \right] a = \sqrt{\gamma} r(t). \quad (A5)$$

The variable a can be obtained from Eq. (A5); then the eddy variables ψ and b are solved.

To solve the cross-stream diffusivity, they consider a passive tracer equation satisfying

$$\frac{\partial}{\partial t}C' + U(z)\frac{\partial}{\partial x}C' + J(\psi, C') + \Gamma_c \frac{\partial}{\partial x}\psi = 0, \quad (A6)$$

where C' is the tracer concentration and Γ_c is the mean tracer gradient. They obtain the solution to C' from Eq. (A6) by assuming C' has the same spatial structure as ψ. Then the cross-stream Eulerian diffusivity can be obtained from

$$\overline{v'C'} = \overline{\frac{\partial\psi}{\partial x}C'} = -\kappa_\perp^E \frac{\partial}{\partial y}\overline{C}. \quad (A7)$$

Their final solution to $\kappa_\perp^E$ in their single-wavenumber mixing model is

$$\kappa_\perp^{single} = \kappa_\perp^E = \frac{k^2}{\kappa^2} \frac{\gamma}{\gamma^2 + k^2[C_w - U(z)]^2} \text{EKE}, \quad (A8)$$

where C_w denotes the wave phase speed

$$C_w = \left(1 - \frac{f}{NH\kappa} \right) U_0 = U_0 - \frac{\Gamma}{N\kappa}, \quad (A9)$$

and EKE is the domain-averaged eddy kinetic energy

$$\text{EKE} = \frac{1}{2}\langle u^2 + v^2 \rangle = \frac{1}{2}\langle |\nabla\psi|^2 \rangle = \frac{1}{4}\mathbb{U}^2 \exp\left(2\frac{N\kappa}{f}z \right). \quad (A10)$$

b. Cross-stream diffusivity from the multiwavenumber theory in the single-wavenumber limit

As shown in Eq. (19), to obtain cross-stream diffusivities from the MW theory, the key is to derive the frequency–wavenumber spectra of cross-stream eddy velocities. In the single-wavenumber scenario from Ferrari and Nikurashin (2010), we can obtain this spectrum from Eqs. (A4) and (A5).

Taking the Fourier transform of Eq. (A4) and multiplying by k^2, we obtain the spectrum for cross-stream (in this case, meridional) velocities:

$$S_v(k',l',\omega') = k^2 S_\psi(k',l',\omega') = \frac{\mathbb{U}^2 k^2}{\kappa^2} \exp\left(2\frac{N\kappa}{f}z \right)|\hat{a}(\omega')|^2 \left| \frac{\delta(k - k', l - l') - \delta(k + k', l + l')}{2} \right|^2, \quad (A11)$$

where $\hat{}$ is the Fourier transform, S_{var} denotes the spectra for variable var, and $|\hat{a}(\omega')|^2$ can be obtained through Fourier transform of Eq. (A5):

$$|\hat{a}(\omega')|^2 = \frac{\gamma|\hat{r}(\omega')|^2}{\gamma^2 + \left[\omega' - k\left(U_0 - \dfrac{\Gamma}{N\kappa}\right)\right]^2}. \quad \text{(A12)}$$

Substituting Eqs. (A11) and (A12) into Eq. (19) gives the cross-stream diffusivities from the MW theory:

$$\kappa_\perp^{\text{multi}} = \frac{1}{4}\frac{\mathbb{U}^2 k^2}{\kappa^2}$$
$$\times \exp\left(2\frac{N\kappa}{f}z\right)\frac{\gamma|\hat{r}(Uk)|^2}{\gamma^2 + \left[Uk - k\left(U_0 - \dfrac{\Gamma}{N\kappa}\right)\right]^2}, \quad \text{(A13)}$$

noting from Eq. (A9) that

$$-(C_w - U)k = \left[Uk - k\left(U_0 - \frac{\Gamma}{N\kappa}\right)\right]. \quad \text{(A14)}$$

Using Eqs. (A14) and (A10), Eq. (A13) can be rewritten as

$$\kappa_\perp^{\text{multi}} = \frac{1}{4}\frac{k^2}{\kappa^2}\frac{\gamma}{\gamma^2 + k^2[C_w - U(z)]^2}[4\text{EKE}|\hat{r}(Uk)|^2]$$
$$= |\hat{r}(Uk)|^2\kappa_\perp^{\text{single}}. \quad \text{(A15)}$$

Recall that $r(t)$ is the white noise forcing with zero mean and autocorrelation $\langle r(t)r*(t')\rangle = \delta(t - t')$; thus, $|\hat{r}(Uk)|^2 = 1$ and $\kappa_\perp^{\text{multi}} = \kappa_\perp^{\text{single}}$. Therefore, in the single-wavenumber limit, the cross-stream diffusivity formula from the MW theory reduces to the single-wavenumber formula from Ferrari and Nikurashin (2010).

APPENDIX B

Derivation of the Multiwavenumber Theory from Tracers and Flux-Gradient Relation

Here, we show that the MW theory from section 2a can also be derived from an Eulerian diffusivity perspective using tracers. The mathematical symbols used below follow the convention of Eulerian diffusivities and apply only in this appendix.

We take the mean and eddy equations for the passive tracer C:

$$\frac{\partial}{\partial t}\overline{C} + \overline{\mathbf{u}} \cdot \nabla\overline{C} - \kappa_0\nabla^2\overline{C} = -\nabla \cdot \overline{\mathbf{F}}, \quad \text{(B1)}$$

and

$$\frac{\partial}{\partial t}C' + (\overline{\mathbf{u}} + \mathbf{u}') \cdot \nabla C' - \kappa_0\nabla^2 C' = -\mathbf{u}' \cdot \nabla\overline{C} + \nabla \cdot \overline{\mathbf{F}}, \quad \text{(B2)}$$

where $\mathbf{u}$ denotes velocity, κ_0 is the molecular or numerical diffusivity of the tracer, and $\mathbf{F}$ is the eddy flux $\mathbf{u}'C'$. Here, $\overline{}$ denotes the ensemble average. For example, $\overline{\mathbf{u}}$ and $\mathbf{u}'$ denote the mean and eddy velocities. We shall use ensemble averages with a suitably large number of ensembles.

If we define the Green's function for each ensemble

$$\left[\frac{\partial}{\partial t} + (\overline{\mathbf{u}} + \mathbf{u}') \cdot \nabla - \kappa_0\nabla^2\right]G(\mathbf{x}, t \,|\, \mathbf{x}', t')$$
$$= \delta(\mathbf{x} - \mathbf{x}')\delta(t - t'), \quad \text{(B3)}$$

we obtain

$$C'(\mathbf{x}, t) = -\int_{\mathfrak{D}}\int_{-\infty}^{t} d\mathbf{x}'\,dt'\,G(\mathbf{x}, t \,|\, \mathbf{x}', t')u_j'(\mathbf{x}', t')\frac{\partial\overline{C}(\mathbf{x}', t')}{\partial x_j'}$$
$$+ \int_{\mathfrak{D}}\int_{-\infty}^{t} d\mathbf{x}'\,dt'\,G(\mathbf{x}, t \,|\, \mathbf{x}', t')\frac{\partial\overline{F}_j}{\partial x_j'}, \quad \text{(B4)}$$

where $\int_{\mathfrak{D}} d\mathbf{x}'$ denotes the integration over the entire available spatial domain $\mathfrak{D}$. From this, we find the ensemble-averaged eddy flux

$$\overline{F}_i = \overline{u_i'C'} = -\int_{\mathfrak{D}}\int_{-\infty}^{t} d\mathbf{x}'\,dt'\,\mathcal{K}_{ij}(\mathbf{x}, t \,|\, \mathbf{x}', t')\frac{\partial\overline{C}(\mathbf{x}', t')}{\partial x_j'}$$
$$+ \int_{\mathfrak{D}}\int_{-\infty}^{t} d\mathbf{x}'\,dt'\,\mathcal{H}_i(\mathbf{x}, t \,|\, \mathbf{x}', t')\frac{\partial\overline{F}_j}{\partial x_j'}, \quad \text{(B5)}$$

where

$$\mathcal{K}_{ij}(\mathbf{x}, t \,|\, \mathbf{x}', t') = \overline{u_i'(\mathbf{x}, t)G(\mathbf{x}, t \,|\, \mathbf{x}', t')u_j'(\mathbf{x}', t')}, \quad \text{(B6)}$$

and

$$\mathcal{H}_i(\mathbf{x}, t \,|\, \mathbf{x}', t') = \overline{u_i'(\mathbf{x}, t)G(\mathbf{x}, t \,|\, \mathbf{x}', t')}. \quad \text{(B7)}$$

This becomes an integral/differential equation for $\overline{\mathbf{F}}$:

$$\overline{F}_i - \int_{\mathfrak{D}}\int_{-\infty}^{t} d\mathbf{x}'\,dt'\,\mathcal{H}_i(\mathbf{x}, t \,|\, \mathbf{x}', t')\frac{\partial\overline{F}_j}{\partial x_j'}$$
$$= -\int_{\mathfrak{D}}\int_{-\infty}^{t} d\mathbf{x}'\,dt'\,\mathcal{K}_{ij}(\mathbf{x}, t \,|\, \mathbf{x}', t')\frac{\partial\overline{C}(\mathbf{x}', t')}{\partial x_j'}. \quad \text{(B8)}$$

The derivation of Eq. (B8) is similar to the derivation of Eq. (2.14) from Kraichnan (1987), which is about

ensemble-averaged eddy flux in a system with zero mean flow and zero κ_0. Note that the widely used standard form of eddy parameterization is

$$\overline{F}_i = -\kappa_{ij}^{\mathrm{E}} \frac{\partial \overline{C}(\mathbf{x}',t')}{\partial x_j'}, \qquad (\mathrm{B9})$$

where κ_{ij}^{E} is the Eulerian diffusivity tensor. Assuming spatial homogeneity, both $\overline{F}_j$ and $\partial \overline{C}(\mathbf{x}',t')/\partial x_j'$ vary slowly spatially; thus, the second term on the left-hand side of the accurate form [Eq. (B8)] is roughly zero, and $\partial \overline{C}(\mathbf{x}', t')/\partial x_j'$ on the right-hand side of the accurate form can be pulled out of the integral. Thus, the accurate form [Eq. (B8)] reduces to the standard form [Eq. (B9)] in the spatially homogeneous case.

In the spatially inhomogeneous case, the accurate form [Eq. (B8)] differs from the standard form [Eq. (B9)]. First, $\overline{F}_i$ from Eq. (B8) depends on both local and nonlocal mean tracer gradients. Second, we need to solve an integral equation for the flux. Though complicated, in principle, for many realizations, we should be able to solve the $G(\mathbf{x}, t \,|\, \mathbf{x}', t')$ equation [Eq. (B3)] numerically and average to find $\mathcal{H}_i(\mathbf{x}, t \,|\, \mathbf{x}', t')$ and $\mathcal{K}_{ij}(\mathbf{x}, t \,|\, \mathbf{x}', t')$.

Now we consider an idealized case. As in section 2a, we assume that 1) the mean flow velocity is much larger than the eddy velocity, that is, $|\overline{\mathbf{u}}| \gg |\mathbf{u}'|$, and that 2) the spatial scales of the mean flow and eddy flux are much larger than the eddies; in other words, the system is approximately spatially homogeneous. Our assumption of homogeneity implies that $|\overline{\mathbf{u}}|$ is constant. We also assume that κ_0 in Eq. (B1) is small. Under the small eddy amplitude and small κ_0 assumptions, Eq. (B3) is reduced to

$$\left(\frac{\partial}{\partial t} + \overline{\mathbf{u}} \cdot \mathbf{\nabla} \right) G'(\mathbf{x}, t \,|\, \mathbf{x}', t') = \delta(\mathbf{x} - \mathbf{x}') \delta(t - t'). \qquad (\mathrm{B10})$$

For small enough excursions, the mean flow is roughly a constant, and thus we obtain

$$G'(\mathbf{x}, t \,|\, \mathbf{x}', t') = \delta[\mathbf{x} - \mathbf{x}' - (t - t')\overline{\mathbf{u}}] \cdot \mathbb{H}(t - t'), \qquad (\mathrm{B11})$$

where $\mathbb{H}$ is the Heaviside step function. Under the spatially homogeneous assumption, $\mathbf{\nabla} \cdot \overline{\mathbf{F}}$ is negligible and $\partial \overline{C}(\mathbf{x}', t')/\partial x_j'$ is roughly a constant; thus, the eddy flux formula [Eq. (B5)] is reduced to

$$\overline{F}_i = \overline{u_i' C'} = -\frac{\partial \overline{C}}{\partial x_j} \left[\iint_{\mathfrak{D}} \int_{-\infty}^{t} d\mathbf{x}' \, dt' \, \mathcal{K}_{ij}(\mathbf{x}, t \,|\, \mathbf{x}', t') \right]. \qquad (\mathrm{B12})$$

Therefore, in this idealized case, the Eulerian eddy diffusivity, defined by the widely used formula [Eq. (B9)], is

$$\kappa_{ij}^{\mathrm{E}} = \iint_{\mathfrak{D}} \int_{-\infty}^{t} d\mathbf{x}' \, dt' \, \mathcal{K}_{ij}(\mathbf{x}, t \,|\, \mathbf{x}', t'). \qquad (\mathrm{B13})$$

Substituting Eqs. (B6) and (B11) into Eq. (B13) leads to

$$\kappa_{ij}^{\mathrm{E}} = \int_{-\infty}^{t} \overline{u_i'(\mathbf{x}, t) u_j'[\mathbf{x} - (t - t')\overline{\mathbf{u}}, t']} \, dt'. \qquad (\mathrm{B14})$$

Following section 2a(1), we set t to be zero without the loss of generality. Then we obtain from Eq. (B14)

$$\kappa_{ij}^{\mathrm{E}} = \int_{-\infty}^{0} d\tilde{\tau} \, \overline{\mathcal{U}_i'(\mathbf{x}, t)|_{t=0} \mathcal{U}_j'(\mathbf{x}, t)|_{t=\tilde{\tau}}}, \qquad (\mathrm{B15})$$

where $\mathcal{U}_i'(\mathbf{x}, t)$ is defined in Eq. (6). Assuming that the eddy statistics are temporally stationary, we have

$$\kappa_{ij}^{\mathrm{E}} = \frac{1}{2} \int_{-\infty}^{\infty} d\tilde{\tau} \, \overline{\mathcal{U}_i'(\mathbf{x}, t)|_{t=0} \mathcal{U}_j'(\mathbf{x}, t)|_{t=\tilde{\tau}}}. \qquad (\mathrm{B16})$$

Note that $\overline{}$ here denotes the ensemble average, which is essentially the same as $\langle \cdot \rangle$ in the main text. Therefore, κ_{ij}^{E} from Eq. (B16) is the same as $\kappa_{ij}^{L,\infty}$ from Eq. (8). Following the derivation from sections 2a(2) and 2a(3), we will obtain the multiwavenumber formulas for the diffusivity tensor [Eqs. (16) and (17)] and cross-stream diffusivities [Eqs. (19) and (20)].

REFERENCES

Abernathey, R., and J. Marshall, 2013: Global surface eddy diffusivities derived from satellite altimetry. *J. Geophys. Res. Oceans,* **118,** 901–916, doi:10.1002/jgrc.20066.

——, D. Ferreira, and A. Klocker, 2013: Diagnostics of eddy mixing in a circumpolar channel. *Ocean Modell.,* **72,** 1–16, doi:10.1016/j.ocemod.2013.07.004.

Bachman, S., and B. Fox-Kemper, 2013: Eddy parameterization challenge suite I: Eady spindown. *Ocean Modell.,* **64,** 12–28, doi:10.1016/j.ocemod.2012.12.003.

Banyte, D., M. Visbeck, T. Tanhua, T. Fischer, G. Krahmann, and J. Karstensen, 2013: Lateral diffusivity from tracer release experiments in the tropical North Atlantic thermocline. *J. Geophys. Res. Oceans,* **118,** 2719–2733, doi:10.1002/jgrc.20211.

Bates, M., R. Tulloch, J. Marshall, and R. Ferrari, 2014: Rationalizing the spatial distribution of mesoscale eddy diffusivity in terms of mixing length theory. *J. Phys. Oceanogr.,* **44,** 1523–1540, doi:10.1175/JPO-D-13-0130.1.

Bretherton, F. P., 1966: Critical layer instability in baroclinic flows. *Quart. J. Roy. Meteor. Soc.,* **92,** 325–334, doi:10.1002/qj.49709239302.

Chen, R., 2013: Energy pathways and structures of oceanic eddies from the ECCO2 state estimate and simplified models. Ph.D. thesis, Massachusetts Institute of Technology and Woods Hole Oceanographic Institution Joint Program, 206 pp.

——, J. L. McClean, S. T. Gille, and A. Griesel, 2014: Isopycnal eddy diffusivities and critical layers in the Kuroshio Extension from an eddying ocean model. *J. Phys. Oceanogr.,* **44,** 2191–2211, doi:10.1175/JPO-D-13-0258.1.

——, and G. R. Flierl, 2015: The contribution of striations to the eddy energy budget and mixing: Diagnostic frameworks, and results in a quasi-geostrophic barotropic system with mean flow. *J. Phys. Oceanogr.,* in press.

——, ——, and C. Wunsch, 2015: Quantifying and interpreting striations in a subtropical gyre: A spectral perspective. *J. Phys. Oceanogr.,* **45,** 387–406, doi:10.1175/JPO-D-14-0038.1.

Danabasoglu, G., and J. Marshall, 2007: Effects of vertical variations of thickness diffusivity in an ocean general circulation model. *Ocean Modell.,* **18,** 122–141, doi:10.1016/j.ocemod.2007.03.006.

Davis, R., 1987: Modelling eddy transport of passive tracers. *J. Mar. Res.,* **45,** 635–666, doi:10.1357/002224087788326803.

——, 1991: Observing the general circulation with floats. *Deep-Sea Res.,* **38A** (Suppl. 1), S531–S571, doi:10.1016/S0198-0149(12)80023-9.

Farneti, R., T. L. Delworth, A. J. Rosati, S. M. Griffies, and F. Zeng, 2010: The role of mesoscale eddies in the rectification of the Southern Ocean response to climate change. *J. Phys. Oceanogr.,* **40,** 1539–1557, doi:10.1175/2010JPO4353.1.

Feddersen, F., 2004: Effect of wave directional spread on the radiation stress: Comparing theory and observations. *Coastal Eng.,* **51,** 473–481, doi:10.1016/j.coastaleng.2004.05.008.

Ferrari, R., and M. Nikurashin, 2010: Suppression of eddy diffusivity across jets in the Southern Ocean. *J. Phys. Oceanogr.,* **40,** 1501–1519, doi:10.1175/2010JPO4278.1.

——, and C. Wunsch, 2010: The distribution of eddy kinetic and potential energies in the global ocean. *Tellus,* **62A,** 92–108, doi:10.1111/j.1600-0870.2009.00432.x.

Firing, Y. L., T. K. Chereskin, and M. R. Mazloff, 2011: Vertical structure and transport of the Antarctic Circumpolar Current in Drake Passage from direct velocity observations. *J. Geophys. Res. Oceans,* **116,** C08015, doi:10.1029/2011JC006999.

Flierl, G. R., and D. J. McGillicuddy, 2002: Mesoscale and submesoscale physical–biological interactions. *Biological-Physical Interactions in the Sea,* M. N. Hill et al., Eds., The Sea—Ideas and Observations on Progress in the Study of the Seas, Vol. 12, John Wiley and Sons, 113–185.

Fox-Kemper, B., and D. Menemenlis, 2008: Can large eddy simulation techniques improve mesoscale rich ocean models? *Ocean Modeling in an Eddying Regime, Geophys. Monogr.,* Vol. 177, Amer. Geophys. Union, 319–337, doi:10.1029/177GM19.

Gille, S. T., and Coauthors, 2012: The diapycnal and isopycnal mixing experiment: A first assessment. *CLIVAR Exchanges,* No. 58, International CLIVAR Project Office, Southampton, United Kingdom, 46–48.

Green, J. S. A., 1970: Transport properties of the large-scale eddies and the general circulation of the atmosphere. *Quart. J. Roy. Meteor. Soc.,* **96,** 157–185, doi:10.1002/qj.49709640802.

Griesel, A., S. T. Gille, J. Sprintall, J. L. McClean, and M. E. Maltrud, 2009: Assessing eddy heat flux and its parameterization: A wavenumber perspective from a 1/10° ocean simulation. *Ocean Modell.,* **29,** 248–260, doi:10.1016/j.ocemod.2009.05.004.

——, ——, ——, ——, J. H. LaCasce, and M. E. Maltrud, 2010: Isopycnal diffusivities in the Antarctic Circumpolar Current inferred from Lagrangian floats in an eddying model. *J. Geophys. Res.,* **115,** C06006, doi:10.1029/2009JC005821.

——, J. L. McClean, S. T. Gille, J. Sprintall, and C. Eden, 2014: Eulerian and Lagrangian isopycnal eddy diffusivities in the Southern Ocean of an eddying model. *J. Phys. Oceanogr.,* **44,** 644–661, doi:10.1175/JPO-D-13-039.1.

Griffies, S. M., 1998: The Gent–McWilliams skew flux. *J. Phys. Oceanogr.,* **28,** 831–841, doi:10.1175/1520-0485(1998)028<0831:TGMSF>2.0.CO;2.

Haine, T. W. N., and J. Marshall, 1998: Gravitational, symmetric, and baroclinic instability of the ocean mixed layer. *J. Phys.*

Oceanogr., **28,** 634–658, doi:10.1175/1520-0485(1998)028<0634:GSABIO>2.0.CO;2.

Holloway, G., 1986: Estimation of oceanic eddy transports from satellite altimetry. *Nature,* **323,** 243–244, doi:10.1038/323243a0.

Holmes-Cerfon, M., O. Bühler, and R. Ferrari, 2011: Particle dispersion by random waves in the rotating Boussinesq system. *J. Fluid Mech.,* **670,** 150–175, doi:10.1017/S0022112010005240.

Johnson, T. J., R. H. Stewart, C. K. Shum, and B. D. Tapley, 1992: Distribution of Reynolds stress carried by mesoscale variability in the Antarctic Circumpolar Current. *Geophys. Res. Lett.,* **19,** 1201–1204, doi:10.1029/92GL01287.

Killworth, P. D., 1997: On the parameterization of eddy transfer. Part 1: Theory. *J. Mar. Res.,* **55,** 1171–1197, doi:10.1357/0022240973224102.

——, and C. W. Hughes, 2002: The Antarctic Circumpolar Current as a free equivalent-barotropic jet. *J. Mar. Res.,* **60,** 19–45, doi:10.1357/002224002762341230.

Klocker, A., and R. Abernathey, 2014: Global patterns of mesoscale eddy properties and diffusivities. *J. Phys. Oceanogr.,* **44,** 1030–1046, doi:10.1175/JPO-D-13-0159.1.

——, R. Ferrari, and J. H. LaCasce, 2012a: Estimating suppression of eddy mixing by mean flows. *J. Phys. Oceanogr.,* **42,** 1566–1576, doi:10.1175/JPO-D-11-0205.1.

——, ——, ——, and S. Merrifield, 2012b: Reconciling float-based and tracer-based estimates of eddy diffusivities. *J. Mar. Res.,* **70,** 569–602, doi:10.1357/002224012805262743.

Koszalka, I. M., and J. H. LaCasce, 2010: Lagrangian analysis by clustering. *Ocean Dyn.,* **60,** 957–972, doi:10.1007/s10236-010-0306-2.

Kraichnan, R. H., 1987: Eddy viscosity and diffusivity: Exact formulas and approximations. *Complex Syst.,* **1,** 805–820.

LaCasce, J. H., R. Ferrari, J. Marshall, R. Tulloch, D. Balwada, and K. Speer, 2014: Floats-derived isopycnal diffusivities in the DIMES experiment. *J. Phys. Oceanogr.,* **44,** 764–780, doi:10.1175/JPO-D-13-0175.1.

Large, W. G., J. C. McWilliams, and S. C. Doney, 1994: Oceanic vertical mixing: A review and a model with nonlocal boundary layer parameterization. *Rev. Geophys.,* **32,** 363–403, doi:10.1029/94RG01872.

Ledwell, J. R., A. J. Watson, and C. S. Law, 1998: Mixing of a tracer in the pycnocline. *J. Geophys. Res.,* **103,** 21 499–21 529, doi:10.1029/98JC01738.

——, L. Laurent, J. B. Girton, and J. M. Toole, 2011: Diapycnal mixing in the Antarctic Circumpolar Current. *J. Phys. Oceanogr.,* **41,** 241–246, doi:10.1175/2010JPO4557.1.

Maximenko, N. A., B. Bang, and H. Sasaki, 2005: Observational evidence of alternating zonal jets in the World Ocean. *Geophys. Res. Lett.,* **32,** L12607, doi:10.1029/2005GL022728.

Morrow, R., J. Church, R. Coleman, D. Chelton, and N. White, 1992: Eddy momentum flux and its contribution to the Southern Ocean momentum balance. *Nature,* **357,** 482–484, doi:10.1038/357482a0.

Naveira-Garabato, A. C., R. Ferrari, and K. Polzin, 2011: Eddy stirring in the Southern Ocean. *J. Geophys. Res.,* **116,** C09019, doi:10.1029/2010JC006818.

Plumb, R. A., and J. D. Mahlman, 1987: The zonally averaged transport characteristics of the GFDL general circulation/transport model. *J. Atmos. Sci.,* **44,** 298–327, doi:10.1175/1520-0469(1987)044<0298:TZATCO>2.0.CO;2.

Pratt, L. J., I. I. Rypina, T. M. Ozgokmen, P. Wang, H. Childs, and Y. Bebieva, 2014: Chaotic advection in a steady, three-dimensional, Ekman-driven eddy. *J. Fluid Mech.,* **738,** 143–183, doi:10.1017/jfm.2013.583.

Randel, W. J., and I. M. Held, 1991: Phase speed spectra of transient eddy fluxes and critical layer absorption. *J. Atmos. Sci.,* **48,** 688–697, doi:10.1175/1520-0469(1991)048<0688:PSSOTE>2.0.CO;2.

Sheen, K. L., and Coauthors, 2013: Rates and mechanisms of turbulent dissipation and mixing in the Southern Ocean: Results from the Diapycnal and Isopycnal Mixing Experiment in the Southern Ocean (DIMES). *J. Geophys. Res. Oceans,* **118,** 2774–2792, doi:10.1002/jgrc.20217.

Smith, K. S., and J. Marshall, 2009: Evidence for enhanced eddy mixing at middepth in the Southern Ocean. *J. Phys. Oceanogr.,* **39,** 50–69, doi:10.1175/2008JPO3880.1.

Taylor, G. I., 1915: Eddy motion in the atmosphere. *Philos. Trans. Roy. Soc. London,* **A215,** 1–26, doi:10.1098/rsta.1915.0001.

Tulloch, R., and Coauthors, 2014: Direct estimate of lateral eddy diffusivity upstream of Drake Passage. *J. Phys. Oceanogr.,* **44,** 2593–2616, doi:10.1175/JPO-D-13-0120.1.

Venaille, A., G. K. Vallis, and K. S. Smith, 2011: Baroclinic turbulence in the ocean: Analysis with primitive equation and quasigeostrophic simulations. *J. Phys. Oceanogr.,* **41,** 1605–1623, doi:10.1175/JPO-D-10-05021.1.

Watson, A. J., J. R. Ledwell, M. Messias, B. A. King, N. Mackay, M. P. Meredith, B. Mills, and A. C. Garabato, 2013: Rapid cross-density ocean mixing at mid-depths in the Drake Passage measured by tracer release. *Nature,* **501,** 408–411, doi:10.1038/nature12432.

Weisstein, E. W., 2014: Cross-correlation theorem. Wolfram Math-World, accessed 5 October 2014. [Available online at http://mathworld.wolfram.com/Cross-CorrelationTheorem.html.]

Wilkin, J. L., and R. A. Morrow, 1994: Eddy kinetic energy and momentum flux in the Southern Ocean: Comparison of a global eddy-resolving model with altimeter, drifter, and current-meter data. *J. Geophys. Res.,* **99,** 7903–7916, doi:10.1029/93JC03505.

Wortham, C. J., 2013: A multi-dimensional spectral description of ocean variability with applications. Ph.D. thesis, Massachusetts Institute of Technology and Woods Hole Oceanographic Institution Joint Program, 184 pp.

——, and C. Wunsch, 2014: A multidimensional spectral description of ocean variability. *J. Phys. Oceanogr.,* **44,** 944–966, doi:10.1175/JPO-D-13-0113.1.

Wunsch, C., 2010: Toward a midlatitude ocean frequency–wavenumber spectral density and trend determination. *J. Phys. Oceanogr.,* **40,** 2264–2281, doi:10.1175/2010JPO4376.1.

Xu, Y., and L.-L. Fu, 2011: Global variability of the wavenumber spectrum of oceanic mesoscale turbulence. *J. Phys. Oceanogr.,* **41,** 802–809, doi:10.1175/2010JPO4558.1.